Benchmarking a 1 kW hybrid hydrogen fuel cell system

A renewable power supply for unmanned aerial vehicles

by Jonathan Envall

LUND
UNIVERSITY

Thesis for the degree of Master of Science
Thesis advisors: Martin Andersson, Marcus Thern, Marcus Lundgren

To be presented, with the permission of the Faculty of Engineering of Lund University, for public criticism on the online meeting at the Department of Energy Sciences on Tuesday, the 14th of February 2023 at 10:00.

This degree project for the degree of Master of Science in Engineering has been conducted at the Division of Combustion Engines, Department of Energy Sciences, Faculty of Engineering, Lund University.

Supervisors at the Department of Energy Sciences were Martin Andersson and Marcus Thern.

Examiner at Lund University was Jens Klingmann.

The project was conducted in cooperation with the Lund University School of Aviation in Ljungbyhed.

Department of Energy Sciences
Faculty of Engineering
Lund University

ISSN: <0282-1990>
LUTMDN/TMHP-23/5513-SE

Typeset in LaTeX
Lund 2023

Abstract

Unmanned Aerial Vehicles (UAV's) offer great versatility in the tasks that they may perform and they are today used in many sectors. The H24LEO project, administered by the Lund University School of Aviation, aims to develop and demonstrate a hybrid proton-exchange membrane fuel cell-powered UAV to aid in search and rescue operations performed by the Swedish Maritime Administration, and reduce the greenhouse gas emissions compared to similar work performed by helicopters. This master's thesis aims to test the performance and learn about the operation of a physical hybrid fuel cell system before it is integrated in a UAV airframe. A test bench was designed and built where experiments with the fuel cell could be run in a controlled manner. An analysis was also made of the system's strengths and weaknesses, and these were compared to those of battery-electric and combustion-based power supplies.

Due to time constraints of the project and major hardware issues with the fuel cell system, results from the experiments could not be gathered in time for this report. An electrical fault due to bad wiring led to the fuel cell not working properly, and repairs could not be performed within the deadline of the project.

This hybrid fuel cell system should be able to provide 6 % better energy density than a battery-electric system, with the same airframe and propulsion system. The system could however be further optimized by using different hydrogen cylinders. The bulkiness of the system is a limitation, with custom modifications of the fuel cell stack being required to fit in the airframe.

The hybrid fuel cell system should be a valid choice for a UAV, and should be able to provide sufficient power during all stages of flight. It does however offer significantly worse range than that of a combustion-based system. Cold Swedish weather could prove to be a challenge as it might compromise the start-up of the system under sub-zero temperatures.

Sammanfattning

Drönare används idag inom en rad områden. Projektet H24LEO, som drivs av Trafikflygarhögskolan vid Lunds Universitet (TFHS) och är finansierat av Vinnova, har som mål att utveckla och demonstrera en drönare driven av ett hybridiserat vätgasbränslecell-system baserat på PEM-tekniken. Denna drönare har som tilltänkt syfte att kunna erbjuda understöd i så kallade Search and Rescure-uppdrag hos Sjöfartsverket, samt erbjuda minskade växthusgasutsläpp jämfört motsvarande arbete utfört av helikoptrar. Syftet med detta examensarbete är att funktions- och prestandatesta bränslecellssystemet innan det skall integreras i drönaren flygplanskropp. En testbädd designades och konstruerades där bränslecellen skulle kunna testas under kontrollerade förutsättningar. En analys gjordes av systemets för- och nackdelar jämfört med ett batterielektriskt alternativ och ett system baserat på en förbränningsmotor.

På grund av tidsbegränsning i projektutförandet samt stor problematik med bränslecellsystemets funktion kunde resultat från experimenten ej samlas in i tid. Ett tillverkningsfel ledde till skadade sladdar inuti bränslecellen, vilket gjorde att bränslecellen ej fungerade som den skulle. Reparationer kunde ej utföras inom projektets deadline.

Denna hybridiserade vätgasbränslecell bör kunna erbjuda omkring 6 % högre energidensitet än ett batterielektriskt alternativ i samma flygplanskropp och med samma elektrisk drivlina. Det finns samtidigt möjlighet att optimera systemet ytterligare genom att använda andra vätgastankar. Systemet har en relativt stor volym, och i detta projekt krävdes viss modifikation av bränslecellen för att den skulle få plats i drönaren.

En hybridiserad vätgasbränslecell bör vara ett rimligt val för att driva en drönare, och bör kunna producera tillräckligt med effekt under en flygnings samtliga etapper. Räckvidden som uppnås är dock klart sämre än den då en förbränningsmotor används. Kallt väder skulle kunna vara ett problem då detta kan orsaka problem vid uppstart av bränslecellen.

Acknowledgements

This master's thesis project marks the end of my five (and a half) year long education in engineering physics at LTH. It has been refreshing to finish my rather theoretical studies with a practical project, in an area that seems to become more and more relevant every day.

I would like to thank Martin Andersson for all his guidance throughout the project, both with constructive conversations and by staying positive in both high and low moments during the project work. I also want to thank Marcus Thern for sharing his experience and knowledge in performing experimental work, and for his help in guiding my work in the right direction.

I also want to thank Anders Olson at the division of Combustion Engines for finding time to help with setting up hardware, his help has truly been invaluable. Further I want to thank the department of Combustion Engines in general for welcoming me and for providing a great social space. Special thanks to Per Tunestål for fun and interesting lunch conversations.

Further I want to thank Marcus Lundgren at the division of Combustion Engines for taking the role as my lab manager, happily providing assistance whenever I asked.

I want to thank Rohith Maben and Rikard Tyllström at TFHS for their help. To Rohith for all the technical assistance and brainstorming, and to Rikard for creating the project in the first place.

Table of Contents

List of Figures

List of Tables

Nomenclature

Abbreviations

BPP Bipolar plate

DEA Dead-Ended Anode

DMFC Direct Methanol Fuel Cell

DoD Depth of Discharge

HHV Higher Heating Value

ICE Internal Combustion Engine

LEL Lower Explosive Limit

LHV Lower Heating Value

LiPo Lithium Polymer Battery

MEA Membrane Electrode Assembly

MTOW Maximum Takeoff Weight

PEMFC Proton-Exchange Membrane Fuel Cell

SLPM Standard Litres Per Minute

SOFC Solid Oxide Fuel Cell

UAV Unmanned Aerial Vehicle

1. Introduction

H24LEO (pronouced ”halo”) is a project administered by the Lund University School of aviation (Trafikflygarhögskolan, TFHS), financed by Vinnova, the Swedish innovation agency. The project aim is to construct a fixed-wing unmanned aerial vehicle to aid in search and rescue missions. Traditionally this sort of work is performed using helicopters, which are noisy, expensive and heavy emitters of carbon dioxide. In order to reduce the emissions of greenhouse gases, primarily CO_2, the UAV is designed to be electrically powered. Instead of using only batteries, which suffer from relatively low energy density per unit of mass, a hydrogen fuel cell together with a small battery will be used in what is referred to as a hybrid fuel cell system. By continuously converting hydrogen and oxygen into electricity, a steady supply of electrical power can be fed to an electric motor while only emitting water as a by-product. Such a system today has a lower weight per unit of electrical energy compared to modern batteries.

The project is a collaboration between TFHS and the Department of Energy Sciences at the Lund University Faculty of Engineering (LTH). The Energy Sciences department recently upgraded their existing laboratory for combustion engines with a new hydrogen gas supply system, which is built with the purpose of being able to perform hydrogen experiments at the department. This project will be the first to actually use this new system, marking the start of a new chapter in the lab work of the Department of Energy Sciences.

In this thesis the aim is to test the performance of a hybrid hydrogen fuel cell system based on the proton-exchange membrane (PEM) technology, observe its characteristics, and enable an as-smooth-as-possible integration with a UAV airframe. The fuel cell is the 1000W AeroStak 1000LV from H3Dynamics, with a lithium-polymer (LiPo) battery that provides both auxiliary power and power to the motor in a hybrid setup.

1.1. Fuel cells

Fuel cells are devices that convert the chemical energy of a fuel and an oxidizer into electricity via electrochemical reactions [1]. They come in many different types and designs, where the choice of fuel and the choice of electrolyte are the main variables. More details on the working principles of fuel cells will follow later in this report. The main advantages of using fuel cells in UAVs are that greenhouse gas emissions from operation are avoided, and that vibrations and noise leveles are reduced compared to combustion-based power sources [2]. In Table 1.1 is a list of common fuel cell types that have previously been used in literature regarding hydrogen-powered UAVs [3].

Of the three fuel cell types listed in Table 1.1, the proton-exchange membrane fuel cell (PEMFC) is the most widely used in UAVs. The PEMFC-technology available today meets

Table 1.1.: Examples of fuel cell types that are used in UAVs. The PEMFC, the fuel cell type of this project, is highlighted.

Fuel cell type	Fuel	Efficiency (%)	Temp. (°C)	Stack specific power (W/kg)	Specific system power (W/kg)
PEMFC	**Hydrogen**	**40-60**	**30-100**	**>500**	**>150**
DMFC	Methanol or Hydrogen	20-30	20-90	>70	>50
SOFC	Hydrocarbon or Hydrogen	30-50	500-1000	>800	>100

weight requirements for applications where the maximum take-off weight is below 25 kg [2]. Its low operating temperature, combined with a relatively high electrical efficiency and gravimetric power density is what makes it attractive versus other types of fuel cells [3].

1.1.1. Hybridization

PEMFCs can provide a steady power supply at a relatively high electrical efficiency, around 50 %, but lacks somewhat in its performance during dynamic loads i.e. when the required power fluctuates heavily [4][5]. This is due to limitations in the speed of which electro-chemical reactions take place within the cell and in the speed of which mass transport occurs and hydrogen flows. The transient loads during peak power draw may also exceed the maximum power that the fuel cell stack is capable of delivering, resulting in sub-optimal performance of the system. To cope with this, a small battery with a high discharge rate can be connected in parallel with the fuel cell and supply extra power when needed. With proper power flow control this battery can also be charged by the fuel cell when excess power is available and can hence be made relatively small, since the hydrogen supplies most of the total energy. This system is what is referred to as a hybrid fuel cell system.

The size of the battery should be chosen so that enough power is available to perform expected high power activities such as takeoff and acceleration. But since the fuel cell system provides better energy density, the battery should not be too large, as this reduces the payload capacity of the vehicle.

Table 1.2.: Examples of fixed-wing fuel cell UAV designs. MTOW is Maximum Takeoff Weight.

Authors	Org.	Year	FC power (W)	Wing span (m)	MTOW (kg)
Lapeña-Rey et al. [2]	Boeing R&T, Spain	2017	200	4,7	11
Gavrilovic et al. [6]	ISAE-SUPAERO, France	2019	550	3,6	20
Özbek et al. [7]	Eskisehir TU, Turkey	2020	250	2,8	6,5
De Wagter et al. [8]	TU Delft, Netherlands	2020	800	-	-

The hybrid hydrogen fuel cell system introduces complexity in the way that the power flow is controlled. There needs to be some kind of device that distributes the power from the

fuel cell and battery in an appropriate way. Since we want the battery to be as small as possible, it is desired that the fuel cell should be able to charge the battery when there is more power available than is being drawn.

A number of studies have been done where prototypes of hybrid hydrogen fuel cell UAVs have been designed and sometimes built, and some notable ones are listed in Table 1.2.

1.2. Unmanned Aerial Vehicles

A UAV, today often referred to as a drone, is a powered aircraft that can be controlled remotely by a computer or an operator, it does not carry a pilot and therefore relies on remote or autonomous control for its flight. These kinds of vehicles are used for many purposes, both civilian and military, and are made in various sizes and designs. Some applications are surveillance, geographic mapping, and military usage for reconnaissance and combat [9].

Figure 1.1.: A multirotor UAV, in this case with four rotors [10].

The multi-rotor UAV is possibly the most recognisable design, as it is used in the hobby-grade drones that are readily available for consumers [11]. The other common design is the fixed-wing UAV that is more resemblant of a traditional airplane that uses wings to create aerodynamic lift while traveling forward. Which one of these two design styles one should choose depends on the application. The main advantage of a multi-rotor system is the ability to perform vertical takeoff and landing (VTOL), while the fixed-wing UAV longer range thanks to the lift being generated by wings [9]. The airframe that is selected in this project is of the fixed-wing type.

Figure 1.2.: Example of a fixed-wing UAV [12].

2. Method

The bulk of the work behind this thesis is in the design and construction of an experiment setup for testing and bench-marking a hybrid fuel cell system. Practical experiments will be run with this setup in order to test the performance of an actual implementation of a fuel cell. Of special interest are the following points:

- The characteristics of the power flow during different loads, how the battery and fuel cell co-operate.
- The efficiency of the fuel cell, and how this changes with different operating points.
- What the load response looks like under various dynamic loads.

The work will also be used to find the best practices for handling gas cylinders before they are mounted in the airframe. The aim is to learn as much as possible about the system as a whole, thus enabling a successful integration into the UAV.

Apart from the practical work, a literature study of the theory behind fuel cells and of fuel cell stacks was performed. The literature study will introduce the basic workings of fuel cells and fuel cell stacks, and contextualize the choice of a hybrid fuel cell system versus battery-electric and combustion-based alternatives. The main focus area here is the system perspective, what makes a PEMFC work well and which parameters should be taken into account when designing a power supply for a UAV. Factors such as energy density, both gravimetric and volumetric will be investigated, as well as the practical usage of the system. Like refueling and operation under extreme conditions.

3. Airframe and hybrid fuel cell system

For this project the H3Dynamics AeroStak 1000LV (from here on referred to as the AeroStak) fuel cell stack with a 33.3 V, 5200 mA h LiPo battery pack has been selected as the hybrid fuel cell system. The AeroStak is a 1000 W PEMFC that weighs 2.3 kg and the battery weighs 1.1 kg. In order to store fuel on-board the UAV, two 300 bar hydrogen cylinders have been selected. These are so-called *type IV* cylinders, meaning that they consist of a polymer liner (PET in this case) overwrapped by carbon fiber [13]. The most important specifications for the hybrid power supply are listed in Tables 3.1, 3.3, and 3.2. See the appendix for complete specifications.

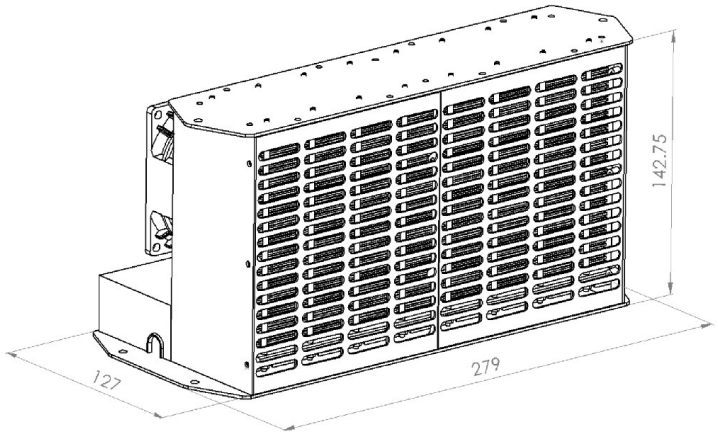

Figure 3.1.: CAD drawing of the AeroStak, from [14]. Dimensions in millimetres. On the top left side one of its two fans is visible. The fans are used to pull air through the stack, enabling cooling and oxygen supply to the cathode.

Table 3.1.: Fuel cell specifications.

AeroStak 1000 LV	
Weight	2.30 kg
Nominal power	1000 W
Ambient airtemp	0 °C–35 °C
Fuel pressure	0.6 – 0.8 bar
Rated electrical efficiency (LHV)	52 %–56 % @ 1080 W

The total weight of the hybrid system is 7.25 kg assuming fully fueled tanks. This leaves 2.75 kg of payload to stay under the MTOW of the airframe, which is 10 kg. See Figure 3.4.

Table 3.2.: Hydrogen tank specifications

HES F2 tanks	
Empty weight	1.58 kg
Pressure regulator mass	305 g
Volume	2 l
Hydrogen mass	42 g
Max pressure	300 bar

Table 3.3.: Battery pack specifications

LiPo Battery	
Weight	1.094 kg
Cell configuration	9 s
C charging	175
C discharging	5
Capacity	5200 mA h
Nominal voltage	33.3 V
Total energy	173 Wh

An estimation of the electrical energy contained within each fuel tank can be calculated using equation 3.1.

$$E_{el} = c_{H_2} \cdot m \cdot \eta \tag{3.1}$$

Where c_{H_2} is the specific energy of for hydrogen, m is the mass, and η is the efficiency of the fuel cell. Using the higher heating value (LHV) of hydrogen as the specific energy, at 120 MJ/kg [15] and an assumed fuel cell efficiency of 50 %, we get E_{el} = 2.517 kJ = 699 Wh per tank. The choice of using the HHV will be further explained in the theory section later on. The total system energy, including the battery, becomes 1563 Wh.

The fuel cell is rated for 1 kW power and we see in table 3.1 that its peak efficiency is achieved roughly at this nominal power, 1080 W. From simulations of the airframe, it is estimated that the UAV will require around 650 W of power while cruising [16], and so it becomes interesting to test what kind of efficiency is achieved at similar power consumption. If the efficiency of the fuel cell is 50 % on average, then the UAV has roughly 2 hours and 24 minutes of flight time. Assumptions about system losses and motor efficiency are included in the estimation of the cruising power draw.

3.1. System operation

During normal operation the fuel cell performs a so-called maintenance cycle every 10 seconds in order to keep the fuel cell membranes in good conditions by removing excess water [14]. The maintenance cycle lasts for 100 ms and during this time the fuel cell

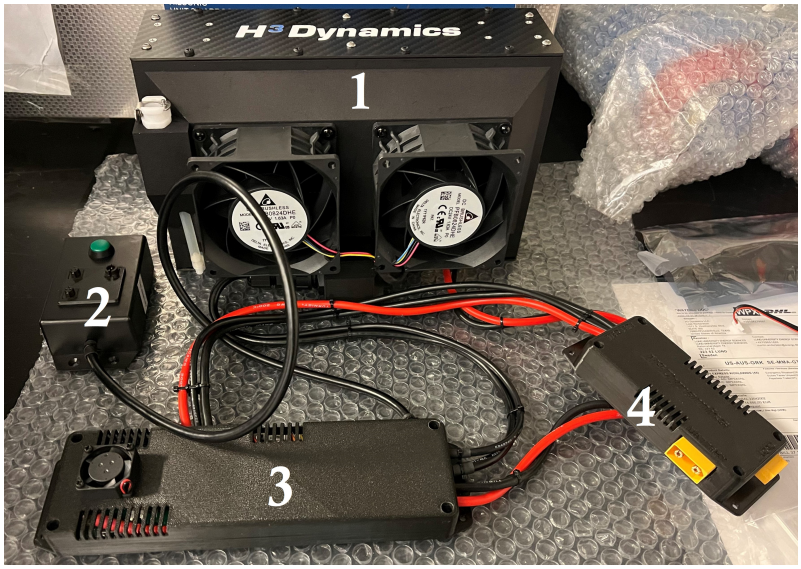

Figure 3.2.: The physical fuel cell stack and electronics. 1: Main stack housing with a white hydrogen quick connect and two fans for coolant/reactant air flow. 2: Start button and connections for telemetry feed and pressure sensors. 3: Logic board. 4: Hybrid card, with battery and load connections. The connector type is XT90.

output is disconnected. This means that the battery must provide 100 % of the power needed during the maintenance cycle and thus it is of extra importance that the battery has a sufficiently high power output. The power output of the battery is also relevant when one wants the aircraft to accelerate quickly. It is expected that over 1.3 kW will be needed during peak load [16] and the motor can draw up to 2.4 kW in short durations [17], this is more than can be supplied by the fuel cell. The battery has a C rating of 175 and at 5200 mAh capacity this gives a maximum discharge current of 910 A.

At nominal voltage this would mean a peak power of 30.3 kW, which is far more than will ever be required by the motor. The system is not dimensioned to handle currents of this magnitude but it shows that the battery is more than capable of providing power both for peaks and for backup to the fuel cell during the maintenance cycle.

The AeroStak is designed for a hybrid system and comes equipped with hardware to manage the power flow of both fuel cell and battery. This is managed via the so-called *hybrid card* which is connected to both fuel cell and battery and distributes power from both sources to the load. The hybrid card also supports charging of the battery mid-operation with a current of up to 1.5 A, enabling charing of the battery while excess power is available from the fuel cell.

In table B.1 one can see that the fuel cell is rated for an ambient air temperature between 0 °C to 35 °C. Especially the lower end of the operating range is of interest for the purpose of the UAV, since the idea is to fly in Swedish climate where sub-zero temperatures are very much expected during the winter months.

C ratings

The C rating is a measure of how quickly a battery can discharge all its stored power. Two batteries with the same maximum discharge current but different capacities will have different C ratings. This is because it will take more time for the larger battery to fully discharge, than for the smaller battery. A C rating of 1 means that it takes 1 hour to fully discharge the battery at max discharge current. For a 5.2 Ah battery this means that the maximum discharge current is 5.2 A. A C rating of 15 means that it take 1/15 of an hour to fully discharge, which in turn means that the maximum discharge current of the 5.2 Ah battery is 5.2 A·15=78 A.

3.2. Integration

The hybridized fuel cell system can be seen as an independent power supply that supplies the UAV speed controller with power. The rest of the system doesn't have to take into consideration if the power comes from the battery or the fuel cell, as long as the total power is sufficiently high.

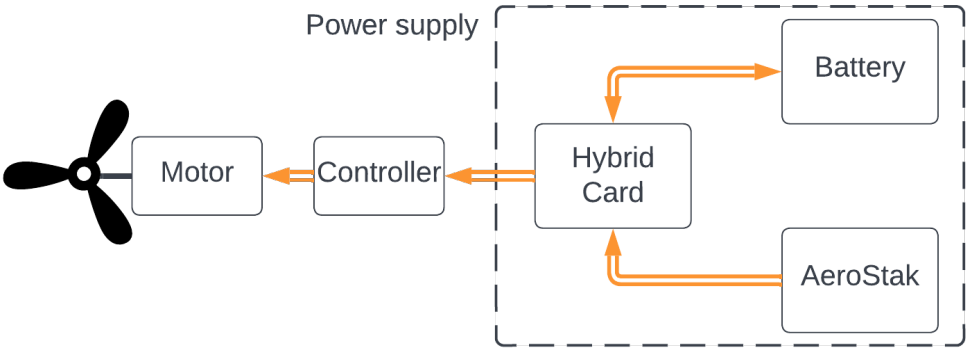

Figure 3.3.: A sketch of the power flow in the UAV propulsion system. The arrows indicate in which directions power is allowed to flow. The dotted line indicates the hybrid fuel cell system, the power supply.

Figure 3.3 depicts the flows of power within the hybrid fuel cell system. The AeroStak supplies power but will not receive any power (except for auxilliary electronics, which are not included in the sketch) while the battery can both supply and receive power. This is to illustrate the charging of the battery. The hybrid card can provide up to 1.5 A of charging current to the battery, which equates to an electrical power of 45 W if the battery is charged to 30 V.

When the hybrid system is up and running, it is a passive component on the UAV system level and does not have to be externally controlled. This makes the electrical integration relatively simple, as the power supply is simply connected using XT90 electrical connectors.

3.3. The Penguin B airframe

Penguin B UAV	
MTOW	21.5 kg
Empty weight	11.5 kg
Wing span	3.3 m
Length	2.3 m
Max payload	10 kg

Figure 3.4.: The Penguin B airframe and its specifications. Empty weight refers to the weight of the airframe, engines, and avionics together.

A model was built by Rohith Maben at TFHS to visualize the physical packaging of the fuel cell system into the airframe. This model used styrofoam shapes as a replacement for the actual fuel cell stack and hydrogen cylinders.

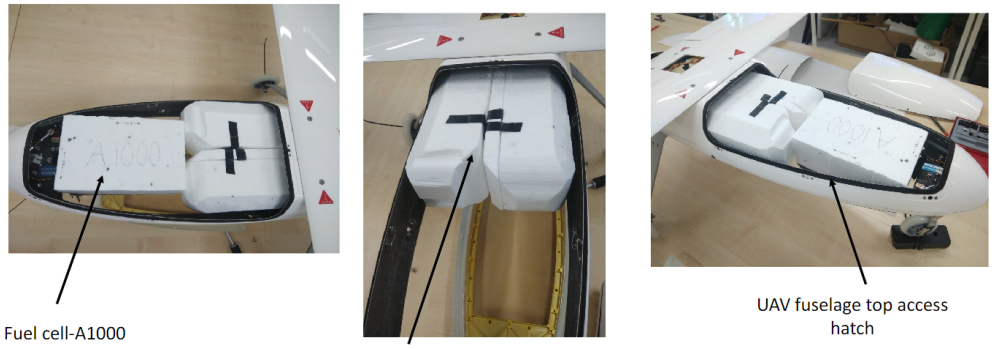

Figure 3.5.: Images of the styrofoam cutouts made to test how the fuel cell system may be integrated in the airframe.

Since the airframe was not specifically designed to fit the hybrid fuel cell system, including the two gas cylinders, the dimensions of the airframe and the AeroStak system were not quite compatible out of the box. In order to be able to fit the hybrid fuel cell system into the airframe, some modifications to the original stack design were ordered from the manufacturer. This included separating the logic board and start button/telemetry connections from the fuel cell stack. In the original design, these components were all included in the same housing as the stack.

Figure 3.6.: The two high pressure cylinders to be used for storing hydrogen onboard the UAV.

4. Fuel cell theory

In this chapter, a brief overview of the principles behind hydrogen fuel cells will be presented. We will start on the basic electrochemical level and then discuss thermodynamics and efficiency. After this we will talk about assembling first a single fuel cell, then a fuel cell stack. Lastly will be an overview of the fuel cell system as a whole, and what affects the performance and life-time of such a system.

4.1. Working principle of PEMFC's

Fuel cells consist of two electrodes, an anode and a cathode, that are separated by an electrolyte. This electrolyte comes in many different variations and can be liquid, solid, or semi-solid. The fuel, the hydrogen gas in the case of the PEMFC, enters the fuel cell at the anode and is oxidized with the help of a catalyst. This separates the H_2 molecule into two protons and two electrons. The protons are able to travel through the electrolyte while the electrons face too much resistance in the electrolyte and instead prefers to travel between the electrodes via an electric circuit, where they perform work if a load is connected [1][18].

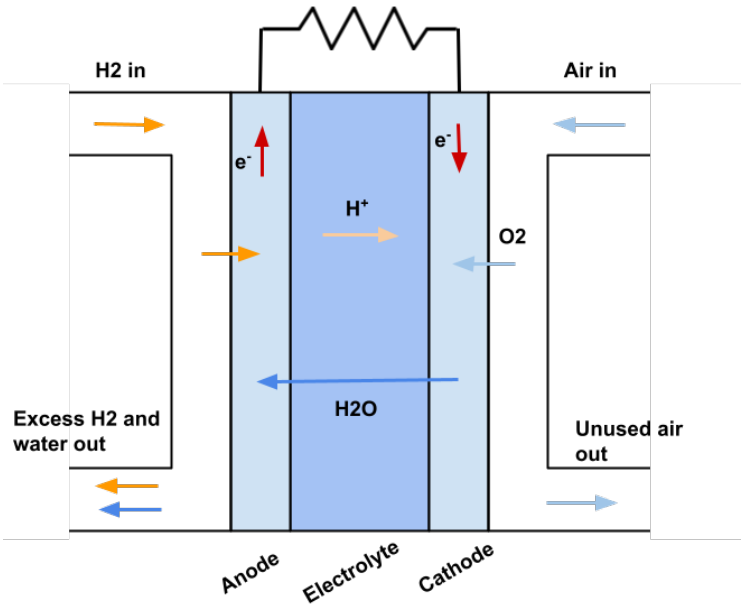

Figure 4.1.: Schematic overview of a hydrogen fuel cell

The electrons eventually reach the cathode where they react together with the protons and oxygen to form water through a reduction. The two half reactions at the anode and cathode

respectively can be written as the following:

$$\textit{Oxidation at anode: } H_2 \rightarrow 2H^+ + 2e^- \tag{4.1}$$

$$\textit{Reduction at cathode: } 2H^+ + 2e^- + \frac{1}{2}O_2 \rightarrow H_2O \tag{4.2}$$

The net reaction for the fuel cell is then:

$$H_2 + \frac{1}{2}O_2 \rightarrow H_2O \tag{4.3}$$

As evident in the chemical equation, water is the only by-product of the hydrogen fuel cell. In practice however not all hydrogen is consumed and therefore there is some release of hydrogen gas apart from the water.

4.2. Thermodynamics and efficiency of fuel cells

The theoretical maximal efficiency of a fuel cell can be formulated as the amount of energy one can possibly extract from the hydrogen fuel, divided by the total amount of energy contained withing the fuel. This is described by the following equation:

$$\eta = \frac{\Delta G}{\Delta H} \tag{4.4}$$

Where η is the efficiency, ΔG is the change in Gibbs free energy caused by the reaction, and ΔH is the corresponding change in enthalpy of the system.

Enthalpy

ΔH is the enthalpy change of the system, with enthalpy (H) referring to the sum of a system's internal energy (U) and the product of its pressure (p) and volume (V). Enthalpy is therefore defined as the following:

$$H = U + pV \tag{4.5}$$

Enthalpy is a measure of the total energy of a system, and therefore the change in enthalpy following a reaction is a measure of how much energy is lost or gained by the system as a result of the reaction. Since the reaction occurs without addition of energy, the change of energy in a fuel cell system will always be negative, meaning that the system loses energy. The amount of energy that the system loses is the maximum amount of energy that could be used for something else, ideally all this energy would become electrical energy that powers the UAV. Since the electrochemical reaction that takes place within the fuel cell has the same product (water) as if the hydrogen and oxygen were to combust, the enthalpy change has the same value as the heating value of hydrogen [19]. This value is different depending on if the product water is in a liquid or a gaseous state. Energy is required for vapour to form, and therefore the enthalpy is lower if the water is gaseous, resulting in the Lower

Heating Value (LHV). If the water is liquid, the value to be used is the Higher Heating Value (HHV). Since the PEMFC operates at a relatively low temperature ($60°C - 80°C$), the product water is liquid and therefore the HHV can be used in calculations [19]. The choice of heating value is however a matter of industry standards and since the AeroStak datasheet efficiency is calculated from the LHV we will also use the LHV in calculations, for consistency.

Gibbs free energy

The Gibbs free energy (G) can be described as the maximum useful work that the system can perform at a constant temperature and pressure. It is the total amount of electrical energy available when hydrogen combines with oxygen in the fuel cell. G depends on the pressure and temperature of the system and will decrease as the system gets hotter and/or as the pressure of the reactants decrease. The change in Gibbs free energy from the reaction is related to the enthalpy change in the following way:

$$\Delta G = \Delta H - T_{ref}\Delta S \tag{4.6}$$

Where ΔH is the change in enthalpy of the system, T_{ref} is the temperature of its surroundings, and ΔS its change of entropy. Enthalpy has previously been discussed, and the term $T_{ref}\Delta S$ can be seen as the 'cost of doing business'. It is irreversibly lost energy of the system which takes the form of heat released by the reaction. We can show this with the following equation for a fuel cell reaction under standard conditions, which are defined as a pressure of 1 atmosphere and a temperature of $25°C$ [19]:

$$H_2 + \frac{1}{2}O_2 \rightarrow H_2O_{liquid} + 237.2 \text{ kJ/mole } \textit{(electricity)} + 48.6 \text{ kJ/mole } \textit{(heat)} \tag{4.7}$$

Just as with the enthalpy change, the change in Gibbs free energy for a system under standard conditions is negative, which is reasonable since Gibbs free energy is partly defined by the enthalpy.

The resulting change in Gibbs free energy is directly proportional to the theoretical potential difference between the two electrodes, i.e. the voltage of the fuel cell. The following relation is true [1]:

$$\Delta G = n_e F E \tag{4.8}$$

Where n_e is the number of moles of electrons, F is Faraday's constant, and E is the voltage of the cell (specifically the potential difference between the anode and cathode).

The Gibbs free energy changes with temperature and pressure, and for an H_2/O_2 fuel cell it can be shown that [18]:

$$\Delta G = \Delta G^0 + RTln\left[\frac{pH_2O}{pH_2p\sqrt{O_2}}\right] \tag{4.9}$$

Where ΔG^0 is the change in Gibbs free energy at standard pressure, which varies with the temperature T of the fuel cell. pH_2, pO_2, and p_{H_2O} are the partial pressures of hydrogen, oxygen, and water vapour, respectively. R is the universal gas constant. One can note that

the Gibbs energy and therefore the efficiency depends logarithmically on the pressure of the reactants and linearly on the temperature of the system. In figures 4.2 and 4.3 we see how the Gibbs free energy changes with regards to temperature and pressure respectively.

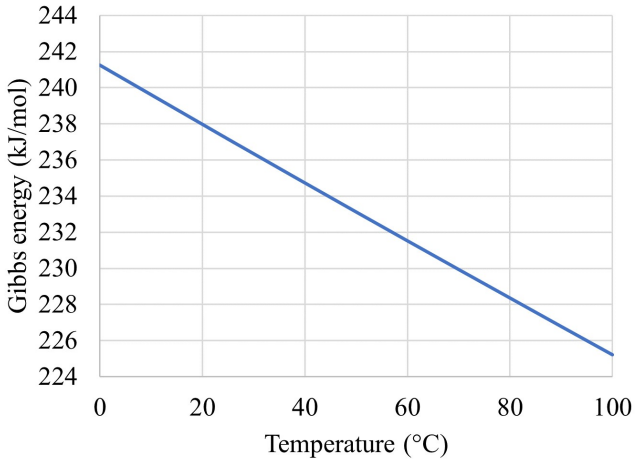

Figure 4.2.: Gibbs free energy as a function of temperature (at standard pressure, 1 bar).

The decrease in the free Gibbs energy as a result of decreased pressure is relatively small and at 4000 metres, where the pressure is roughly 60 % of sea-level pressure [20], less than 1 % of Gibbs free energy is lost. Assuming that the temperature of the system decreases by a few degrees Celsius, which is reasonable since the surrounding temperature decreases with increased altitude [21], relatively small altitude changes will not have major effects on the thermodynamic efficiency. However due to other physical effects the actual efficiency of the system is very likely to decrease [22].

Electrical efficiency

With equation 4.4, we want to calculate the theoretical electrical efficiency of a hydrogen fuel cell. Using standard values for temperature and pressure; a temperature of 295 K

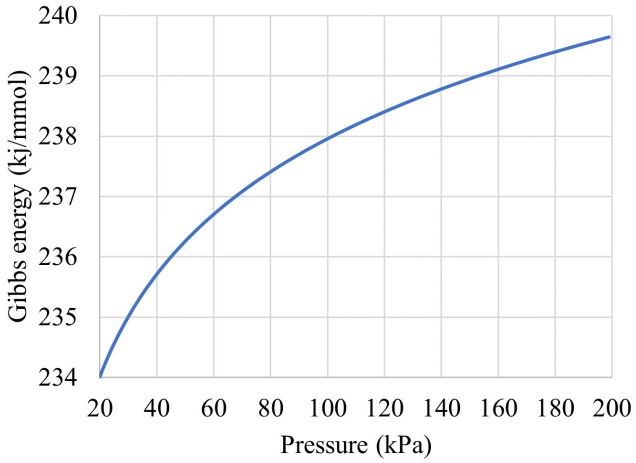

Figure 4.3.: Gibbs free energy as a function of pressure (at 25 °C).

($22^{\circ}C$) and a pressure of 101 kPa (1 atm), we use tabulated values from [1] and get a thermodynamic electrical efficiency of $\eta = 237.98/285.98 = 0.83$. A very high number as far as energy conversion goes. In a practical fuel cell however, this kind of efficiency is not attainable since a number of losses affects the performance. The three most significant losses are activation losses, ohmic losses, and mass transport (or concentration-) losses. The losses result in a decrease in cell voltage, and we can express the total cell voltage according to the following [1]:

$$E_{cell} = E_{cathode} - E_{anode} - (\eta_{act} + \eta_{conc})_{cathode} - (\eta_{act} + \eta_{conc})_{anode} - \eta_{ohm} \quad (4.10)$$

Where:
E_{cell} is the cell voltage.
$E_{cathode/anode}$ is the cathode and anode potential respectively.
η_{act} is the potential drop due to activation losses. This is most significant at low current densities.
η_{ohm} are ohmic losses that occur due to the resistance faced by the ions flowing in the electrolyte and from electrical resistance affecting the electrons.
η_{conc} are mass transport losses that arise from concentration differences between anode and cathode. The mass transport losses are only significant for relatively high current densities [1].

Due to these losses the actual efficiency of a PEMFC ends up at around 50 %. The difference between theoretical efficiency and actual efficiency is obviously very significant. In order to calculate a realistic energy efficiency, it is essential to take the losses into account. But this is not a straight forward task since the losses depend on the physical fuel cell system and its components, as well as the current density at a given power draw. The most convenient way of calculating the actual efficiency of a fuel cell is to compare the total amount of produced energy with the available energy in the hydrogen fuel that is consumed during the same time. This can be expressed like the following:

$$Efficiency = \frac{Energy\ produced\ per\ unit\ of\ H_2\ mass}{Lower\ heating\ value\ (LHV)} \quad (4.11)$$

4.3. Physical assembly

An actual fuel cell needs to be built, and here follows an overview of the components that are typically used when constructing first the cells, later the system.

The part of the fuel cell where the electrochemical reaction take place, as depicted in Figure 4.1, is the so-called membrane electrode assembly (MEA). In the middle of the MEA is the proton exchange membrane (PEM), which is the component that enables protons to travel from anode to cathode, while simultaneously imposing large electrical resistance. The most commonly used material in these types of membranes is the fluoropolymer material Nafion [24]. The membrane is sandwiched between two catalyst layers that enable the reactions at the anode and cathode to take place. Outside each catalyst layer is then a gas diffusion layer placed. The gas diffusion layer is responsible for distributing hydrogen over the PEM surface in an even manner. It must also be able to conduct electricity. In Figure

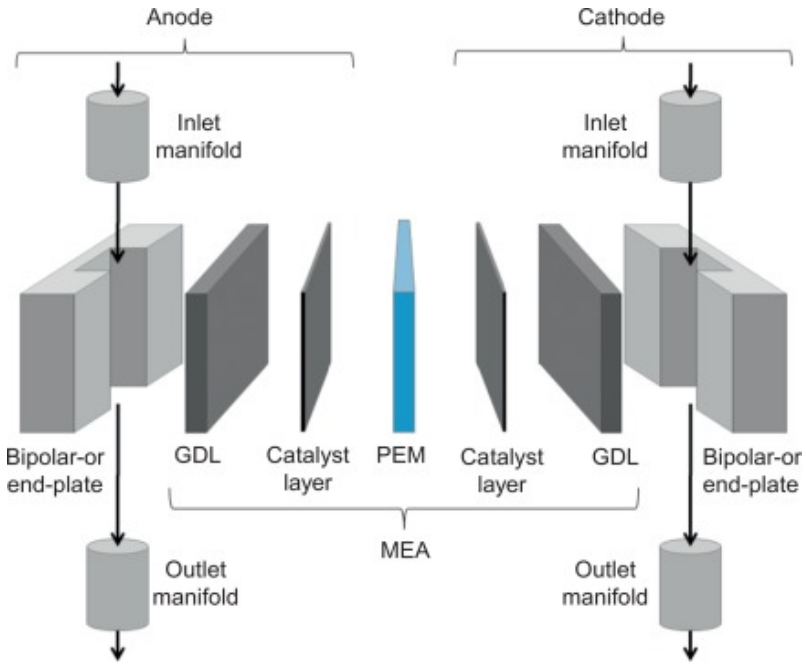

Figure 4.4.: Exploded view of a PEMFC segment, illustrating the MEA and the use of bipolar plates and endplates. Used with permission from [23].

4.4 is an exploded view of a stack segment, illustrating the position of each component.

Multiple MEA's are stacked together to increase the capacity of the fuel cell until the desired output power is reached. To do this one uses so-called bipolar plates (BPP's) in between each MEA. These plates have multiple functions as they are responsible for the conduction of electricity between the MEA's, the conduction of heat from the MEA's to the air (cooling), as well as the distribution of both fuel and air to the MEA's [25]. The rim of these plates are sealed with gaskets to avoid leakage of fuel or oxygen. The stack of MEA's are clamped together with end-plates to improve the electrical conductivity of the stack by reducing the contact resistance of each component [26].

4.4. The fuel cell system

The complete hybrid fuel cell system consists of the fuel cell stack, a fuel supply, the hybrid battery, some form of cooling and oxygen supply, and control electronics. In order to vary the output power of the fuel cell stack, the supply of fuel needs to be controlled at the stack input. A larger flow of fuel means a higher power output and vice verse. This means that there is some delay in how fast a fuel cell can respond to load changes since the flow of gas cannot change instantaneously.

4.4.1. Purging

In order to maximize the hydrogen usage in PEMFC's, it is desirable that as little hydrogen as possible is wasted. The two common design options for PEMFC's where this is

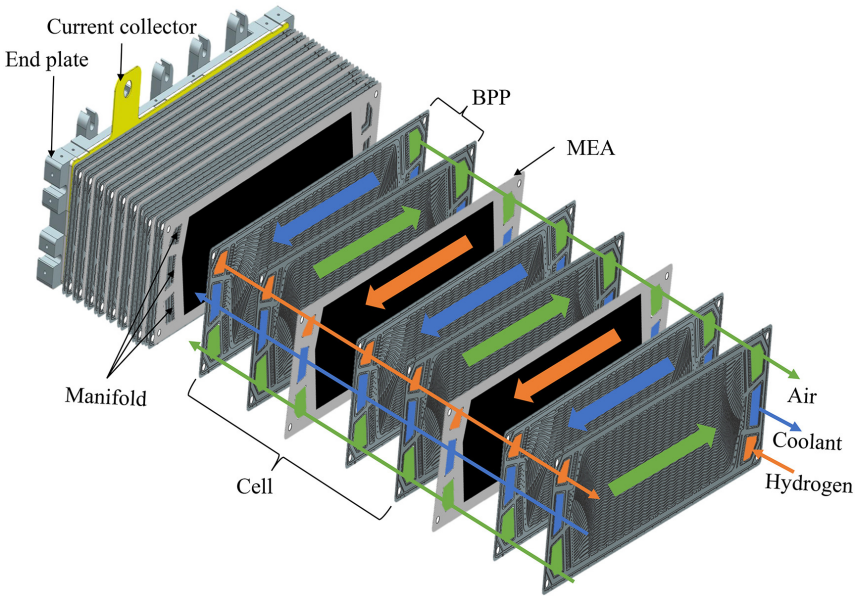

Figure 4.5.: An exploded view of the stack assembly. Multiple MEA's are stacked together between bipolar plates, creating the fuel cell stack. The channels where gases are transported within the stack are also indicated in different colours. The figure depicts a stack assembly with a dedicated cooling system, the AeroStak however does not rely on such a system and is instead cooled by the ambient air that supplies the stack with oxygen [27]. Used with permission from [28].

attempted is either the Dead-Ended Anode (DEA) setup or a design where unused hydrogen is recirculated to the anode inlet. DEA means that the anode exit is closed, and so the hydrogen cannot exit the anode without reacting. Recirculation is simply letting unused hydrogen rejoin with hydrogen from the fuel supply. For both design options one is faced with the risk that both water and various impurities accumulate at the anode, which over time will lead to decreased performance [29]. To deal with this issue, PEMFC's performs regular *purges* to clear the anode, which in practice means letting gas and water leave the anode by opening a valve. The frequency and duration of purging affects the stack voltage and can be optimized for maximal efficiency [30]. With purging, the overall system efficiency can be made greater with a dead-ended anode design compared to an open-ended anode [29].

4.4.2. Membrane humidity and cold starts

The proton-exchange membrane contains liquid water and must be kept humidified in order to not lose performance [14]. This is not an issue during operation as the liquid water produced by the electrochemical reaction humidifies the membrane continuously. Potential issues arise when the fuel cell stack has not been operational for a very long time, since the membranes will slowly dry out if not conditioned regularly. Conditioning simply refers to running the fuel cell for some time so that it produces water that can re-humidify the membranes.

Since there is liquid water present in the fuel cell stack during operation, it becomes

sensitive to low temperatures. Starting a PEMFC at sub-zero temperatures is referred to as a ”cold start”, and is a research area with a lot of focus since cold starts are one of the remaining hurdles for commercial applications of PEMFC's [31][32][33]. If the stack holds a temperature below freezing while starting, there is a risk that the produced water freezes within the pourous layers of the assembly. This freezing can result in loss of performance or even total failure of the startup sequence [33]. The issues are due to ice formations interfering with the transport phenomena within the cell. When the PEMFC is running, the exothermic reaction heats the body of the fuel cell which means that the low temperatures are less of an issue. The AeroStak does not have a preheating system, and therefore is not rated to start below freezing.

4.5. Degradation and lifetime

All fuel cell technologies are subject to various forms of degradation that limits its useful life. The specific types of degradation that occur will vary between different fuel cell technologies, and the number of factors that causes degradation or affects the degradation speed is rather large. However the most important degradation modes and their 'triggers' for PEMFC's are relatively well-documented.
The most sensitive part of a PEM fuel cell is the proton-exchange membrane itself, and it is typically the degradation of the proton-exchange membrane that affects the overall health of the fuel cell the most [34]. Three main modes of degradation can be identified for the membrane:

Mechanical degradation:
Mechanical degradation involves the membrane experiencing creeping or the development of pinholes or cracks [34]. The same study notes that the potential causes for these phenomena are many. Manufacturing defects in the membrane itself may exist, but mechanical stress can also come from improper assembly of the membrane-electrode assembly or inhomogeneous compression of the bipolar plates.

Thermal degradation:
This type of degradation occurs primarily when temperatures reach $200°C$ and is essentially negligible for temperatures below $100°C$ [34]. There is however potential for degradation feedback loops as membrane defects may cause local hotspots via pinholes (mechanical degradation) in the fuel cell where harmful temperature levels may be reached [35].

Chemical degradation:
May be polymer degradation caused by hydroxyl (HOH) and peroxyl (HOOH) radicals [34] or metal cation contamination caused by corrosion of the bipolar plate(s) [36]. In either case these phenomena can cause thinning of both membrane and the catalyst layer.

Apart from these potential membrane issues, there may also occur degradation of the catalyst layer, the gas diffusion layer, the bipolar plate, and the sealing gaskets. Meaning that essentially all components of the fuel cell are susceptible to wear. The deterioration of the catalyst layer is an important culprit when discussing the lifetime of fuel cell applications. The Pt coating experiences sintering and dissolution over time that leads to the decreased efficiency of the fuel cell [34]. These phenomena are irreversible and studies have shown

that the negative effects develop quicker under static loads than under dynamic loads [37]. This does however not mean that it is favorable to have very large power fluctuations as other studies show that large transients will decrease the life-time of the system [38][39].

The life-time of a PEMFC stack can be expected to lay in the range between 500 to 900 hours [38][39], with the end of life defined as the point in time when the fuel cell stack has permanently lost 10 % of its nominal operating voltage. The AeroStak is, as mentioned, rated for 500 hours of operation which is in line with the literature.

5. System comparison

In this chapter an effort is made to lay out the differences and advantages/disadvantages of three common options when it comes to UAV power supplies. A power supply is in this context the system that stores energy and converts it to useful mechanical energy, i.e. the components from the fuel tank or battery to the motor and the components in between. What is commonly referred to as ”tank-to-wheel”. The Penguin B aircraft previously described is selected as the airframe to be powered, resulting in a 650 W power consumption while cruising and 1300 watt during power-demanding situations. For an electric system, two options are considered. Firstly the PEMFC hybrid system, and secondly a battery-only system based on state-of-the art lithium-ion polymer batteries. To put these electric options into perspective, a system based on an internal combustion engine (ICE) is also considered where a small two-stroke gasoline motor, designed specifically for this application, powers the aircraft. The energy supplies are dimensioned to deliver roughly 2.5 hours of flight time (a rather low number for the combustion solution, discussed later) and be able to deliver at least 1500 W during peak load. Unfortunately the exact efficiencies for all the components are not available, instead values for similar systems are used as an approximation.

The energy conversion efficiency for a similar one cylinder two-stroke IC engine is 21 % when operating in proximity of its most efficient power point [40]. The electric motor is assumed to have a 90 % efficiency and it is assumed that the batteries has a discharge efficiency of 95 %. The efficiency of the hybrid fuel cell system have been discussed previously and is assumed to be 50 % relative to the higher heating value. Losses in wires and electric speed controller are not accounted for, but assumed to be negligible.

Table 5.1.: The three power different power supplies which are discussed.

Hybrid PEMFC	LiPo battery	2 stroke engine
AEROSTAK 1000LV 2x HES 2L fuel tanks 5200mAh 33,3V LiPo Brushless motor [17] (the same as this project)	46000mAh LiPo [41] Brushless motor [17]	Skypower SP-28 CR [42] 710 ccm fuel tank [43]

Energy density

It is of great importance that the energy density of the system is sufficiently high, as this parameter effectively limits the range of the UAV. The term energy density here refers to the gravimetric energy density of the energy supply including the losses that follow when converting chemical energy to mechanical energy. This means that the energy density is

calculated ”at the propeller”, so that engine losses are taken into account. The energy content and mass of the hybrid hydrogen system has been introduced in Chapter 3. The mass of the ICE is 1.34 kg and the energy content is calculated with an energy density of gasoline of 12.9 kWh/kg. It is assumed that the mass for gasoline + tank + accessories is 1kg. The energy content of the large battery is estimated to be 1532 Wh and its mass is 7182 g. The electric motor used by the hybrid PEMFC system and the battery-electric system weighs 595g. It turns out that the combustion alternative provides by far the highest amount of energy per unit of system weight, 616 Wh/kg. The number for the battery-electric system is 178 Wh/kg. For the hybrid PEMFC the energy density is 189 Wh/kg. The hybrid PEMFC system thus provides 6 % better energy density than the battery electric option.

It should be noted that the hybrid PEMFC system can be further optimized by using a single larger hydrogen cylinder and designing the airframe specifically to fit this cylinder. Due to the fixed design of the airframe, this was not possible here.

Power

The estimated peak power required at takeoff is estimated to 1300 W. If the power density of the system is too small, it will not be possible for the UAV to take-off. All systems are capable of providing more than enough power and thus the power or power density will not be discussed further here.

Time to recharge

It is valuable to be able to quickly refuel/recharge the power supply of a UAV. This enables a quick turnover, allowing an operator more flexibility when scheduling missions or responding to urgencies. For surveillance and reconnaissance, it might not be absolutely necessary to have the ability of near-instant turnover. But for search and rescue-operations, this could be important. The two fuel-based energy supplies have the capacity for rather quick refueling. For the hybrid PEMFC system it is a matter of minutes [44] for the fueling process. The gasoline tank contains less than one litre of un-pressurized liquid fuel and refueling is clearly very quick. The large battery on the other hand has a C-rating of 5 while charging, meaning that it replenishes its 42 ampere hours in $\frac{42}{5} = 8.4h$ or 8h24m. It is however possible to swap an empty battery with a charged one, resulting in a turnover time similar to the other two options. It is notable that filling hydrogen cylinders to high pressures require some infrastructure, either in the form of stationary cylinders with very high pressure, or in a refueling compressor that pressurizes the gas to the 300 bar that the onboard cylinders can handle. Such compressors are available [45]. Battery charging requires a battery charger, and gasoline refueling is a matter of pouring liquid into the tank.

Life-time

The system lifetime is defined as the number of hours that the system is expected to operate before it is necessary to replace it entirely or perform non-trivial maintenance or repairs.

The combustion engine is far more advanced in this area than the PEMFC, and some major hurdles must be overcome by the fuel cell industry. Because of the relative youth of the PEMFC, not much data is publicly available on the actual lifetime of systems. The selected fuel cell is rated for 500 hours of operation. The lifetime of a LiPo battery is measured in the number of cycles that it can perform and is heavily influenced by the so-called depth-of-discharge (DoD), or how much of the capacity is used on each cycle [46]. As a conservative estimate 300 cycles have been used, which would allow for near 100 % DoD on each cycle, and around 700 hours of flight. The lifetime of the ICE is in the 1000's of hours [42].

Physical size

When engineering the complete UAV package, it becomes of interest how large is the physical space taken up by the energy supply. A small system results in easier packaging and potential for bulkier payloads. The combustion alternative is the smallest at 3 dm^3, with the battery-electric option close behind at 3.6 dm^3. Due to the large hydrogen cylinders of the hybrid hydrogen fuel cell system, the physical size of this system is, at 13 dm^3, far larger than the other two alternatives. For this system it is effectively its size that limits the energy density as it is difficult to fit additional cylinders in the airframe. One additional cylinder would result in a system energy density of 232 Wh/kg, at a system mass of 9.17 kg. A 22 % increase. This is within the MTOW of the airframe but is not practically possible due to the space constraints. This is in contrast to the battery-electric alternative where mass is the limiting factor. For the combustion alternative, it is possible to fit a much larger tank to achieve longer flight time. With a ten times larger (7 liter) fuel tank, the system gets a 10-fold increase in total energy and a 3 times greater energy density (1938 Wh/kg). This system would have roughly the same mass as the hybrid fuel cell system (7.3 kg), but with still a lower volume (roughly 10 dm^3 assuming a density of 0.75 kg/dm^3 for gasoline).

Table 5.2.: Overview of the three different systems and the parameters that have been discussed in this section.

	Hybrid PEMFC	**LiPo battery**	**2 stroke engine**
Energy content	1.72 kWh	1.28 kWh	1.44 kWh
Mass	7.84 kg	7.18 kg	2.34 kg
Energy density	189 Wh/kg	178 Wh/kg	616 Wh/kg
Refuel/-charge time	~ 10 minutes (temperature dependent [44])	8h24m @ 5C charge rate. Possibility of swapping batteries.	A few seconds to refill gas tank.
Expected lifetime	500 h	~ 700 h with 300 expected cycles.	1000's of hours [42].
Physical volume	13 dm^3	3.6 dm^3	3 dm^3

6. Experimental work

6.1. Test bench

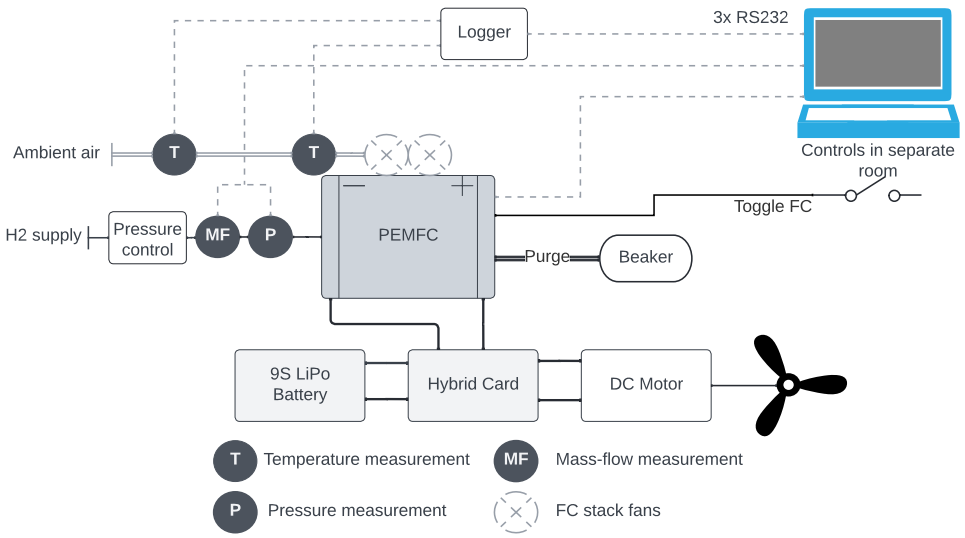

Figure 6.1.: A schematic overview of the experiment setup.

A test bench for the fuel cell system was designed and implemented in one of the lab cells at the department of energy sciences at the faculty of engineering at Lund University. The goal of the test bench was to have a simple design that did not require the manufacturing of custom parts. But still a design that can perform the required measurements and is easily controlled. A schematic overview of the final setup can be seen in Figure 6.1.

There are multiple measurements being made simultaneously and this data is streamed on three separate RS232 channels to the controlling PC. These are the three data streams:

Fuel cell data feed
The AeroStak measures a large number of parameters and provides some diagnostic and debug output as well. The format of the data row that is transmitted by the AeroStak can be seen in Table 6.1.

Mass flow controller data
Both hydrogen mass flow and hydrogen pressure are monitored by two mass flow controllers. These are set to polling mode which means that the PC asks for the data, and the controllers respond individually with the measurements.

Ambient temperature data

Two temperature probes provides ambient air temperature readings. The measurements are made by a data logger which is polled by the PC for the data.

The fuel cell stack performs continuous measurements of various physical parameters. Notably the current flow from the fuel cell and to/from the battery is measured by the stack. Stack voltage and battery voltage are two other important parameters that the stack monitors. These measurements are performed at a rate of roughly 1 Hz. A complete list of the data that is transmitted by the stack is available in Table 6.1.

Stack Voltage	[V]
Load Current	[A]
Power	[W]
Energy	[Wh]
Battery Voltage	[V]
Battery Current	[A]
Load Voltage	[V]
Temperature 1	[$^{\circ}C$]
Temperature 2	[$^{\circ}C$]
Temperature 3	[$^{\circ}C$]
Temperature 4	[$^{\circ}C$]
Stack Pressure	[bar]
Tank 1 Pressure	[bar]
Tank 2 Pressure	[bar]
Board Temp	[$^{\circ}C$]
Fan Speed	[%]
State	-

Table 6.1.: The data fields contained within the AeroStak telemetry, in the same order as they are transmitted.

The AeroStak outputs this data continously on a serial bus. Since the UAV will be airborne, it is required that this data can be transmitted wirelessly so that the telemetry can be recorded during flights. For this purpose, H3Dynamics provided a wireless data link via two 433 MHz transceivers. One of the transceivers connects to the data stream and the other to the monitoring PC. In order to verify the wireless function, this system was also used in the test bench. The receiving transceiver outputs the data in a serial format that is read via USB.

6.1.1. Mass flow measurements

The mass flow and pressure measurements are made by the Alicat MC 100SLPM mass flow controller. This device uses laminar differential pressure to calculate a standardized mass flow rate [47]. This means that the device first converts a turbulent gas flow to a laminar one, using a laminar flow element. When the flow is laminar, the pressure drop

Figure 6.2.: The two wireless transceivers used to transmit telemetry data from the AeroStak to the controller PC.

over a flow channel is measured and this can be used to calculate a volumetric flow rate using the Poiseuille equation:

$$\text{Volumetric flow} = (P_1 - P_2)\pi r^4 / 8\eta L \tag{6.1}$$

Where:
P_1 is the static pressure at the inlet.
P_2 is the static pressure at the outlet.
r is the hydraulic radius of the restricton.
η is the absolute viscosity of the gas.
L is the length of the restriction.

The device then calculates the mass flow by correcting the volumetric flow for temperature, pressure, and gas compressibility.

No mass flow controller was available where a calibration had been performed recently. To lower the risk of calibration-related measurement errors, two mass flow controllers were used in series during the tests, if little difference were to be found between the measurements of the two controllers, one could be more confident in the accuracy of the measurements.

The two mass flow controllers were connected to an Alicat BB9-232 breakout box, Figure 6.4, which is essentially a multiplexer that allows two devices to share the same serial bus. The breakout box also provides power to the devices. The mass flow controllers are polled for data by the controllig PC using individual IDs.

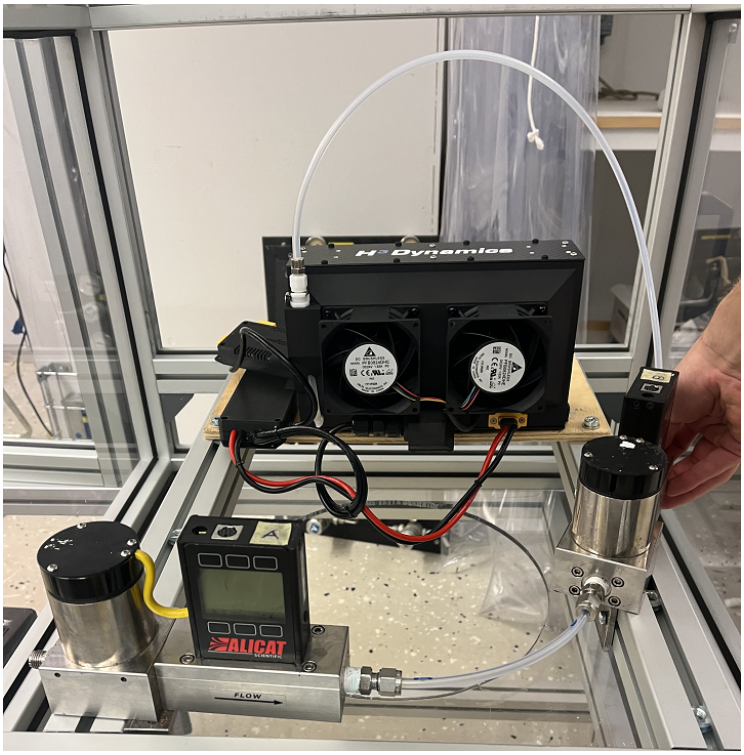

Figure 6.3.: The installed mass flow controllers, with the AeroStak in the background.

6.1.2. Temperature measurements

The air temperature is measured with two PT1000 probes connected to an Agilent 34970A data logger. The PT1000 probes changes their electrical resistance linearly depending on the temperature, and are calibrated to have a resistance of 1000 Ω at $0°C$. The data logger is polled every 5 seconds by the controlling PC, which triggers it to measure the resistances of the two probes, and convert the value into the corresponding temperature. These values are transmitted on the serial bus.

No equipment for accurately varying the temperature within the test cell was available. But in order to examine the effects of temperature, the experiment setup can be taken outdoors where the air is colder.

6.1.3. Data collection and monitoring

In order to monitor and log this data simultaneously, a LabView program was developed specifically for the task. An image of the LabView front panel can be seen in Figure 6.5 below. The block diagram can be found in the appendix. The program allows the user to monitor the data in real-time and to stop the gas flow if necessary. The program produces a TDMS file with all the acquired data as well as a text file with the entire log output of the 1000LV. The LabView program features a number of charts and indicators which makes it possible to monitor the power consumption, fuel flow and pressure, temperature, and more parameters while experiments are running. It is also possible via the interface to start and stop the gas flow, by instructing the mass flow controller(s) to do so via the serial

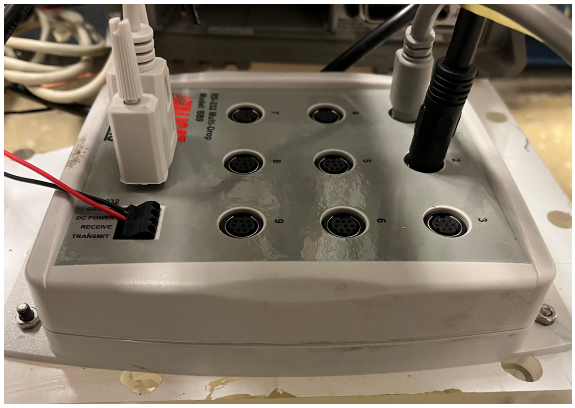

Figure 6.4.: The BB9-232 multiplexer for communicating with two mass flow controllers simultaneously. Visible is the power connection (red and black wire), the RS232 connector, and the two mass flow controller connectors.

connection.

6.1.4. Electrical load

An air brake was used to load the hybrid fuel cell system. This consisted of a propeller connected to a DC motor, controlled by an electronic speed controller. This was the same type of motor and controller meant to later be used in the actual UAV, which was advantageous since it meant that the test-bench loads will be more or less identical to the actual loads in the UAV. The components of the air brake system are listed in table 6.2 below.

Table 6.2.: List of load components.

DC motor	Hacker A60-5S V4 28-Pole kv295
Propeller	20 X 10 E
Speed controller	JETI Spin 125 Opto
Controlling device	FlySky FS-T6

Table 6.3.: Equipment used for the lab setup

What?	**Device**	**Qty**
Mass flow and pressure measurements	Alicat MC 100SLPM	2
RS232 Multiplexer	Alicat BB9-232	1
Air temperature sensor	PT1000 probe	2
Air temperature logging/streaming	Agilent 34970A	1
Hydrogen sensor	Evikon E2608-LEL	1
Multimeter for monitoring H_2 sensor	Agilent 34401A	1
Computer connection	RS232 to USB adapter	3
	RS232 cables	3
Power to electronics	Power supply	2

Figure 6.5.: LabView front panel.

6.1.5. Hydrogen supply

The hydrogen for the experiments was stored in an industrial 150 bar 50 litre cylinder in the lab's gas storage building. Piping runs from the storage into the lab cell, transporting the hydrogen at up to 15 bar. In the lab cell the gas pressure is regulated down to operating pressure via a pressure regulator positioned just before the gas connection.

6.2. Load profiles

A number of different load profile cases were chosen in order to test the performance of the stack during different operating conditions. Of special interest is the performance at cruising power, and the characteristics of the fuel cell during transient loads. A power sweep was to be performed where the voltage and current of the stack was monitored while varying the load from 0 to the maximum fuel cell power output. From this data it is possible to create a plot that displays the voltage and current characteristics of the stack, an IV-curve. Combining the power readings with the corresponding mass flow measurements makes it possible to calculate the efficiency for various power draws. This is useful since the efficiency readings makes it possible to calculate the range of the UAV at different cruising power.

Figure 6.6.: The DC motor and the RC controller used as the electric load and for controlling said load, respectively.

6.3. Measuring efficiency

As discussed earlier, the efficiency of a fuel cell stack can be calculated by comparing the amount of consumed fuel to the energy produced by the fuel cell. The unit of mass that is measured during the experiments is the mass flow, the time derivative of the consumed hydrogen. In order to continuously calculate the efficiency, the time derivative of electrical energy (electrical power) has to be used. This looks like the following:

$$\eta_{FC} = \frac{P_{el}}{\dot{m}_{H_2} \cdot HHV} \tag{6.2}$$

Where P_{el} is the electrical power, $\dot{m}_{H^2}$ is the mass flow of hydrogen, and HHV is the Higher Heating Value of hydrogen.

6.4. System behaviour without fuel supply

During flight it is possible that the aircraft runs out of fuel before having returned to base. This could be because of an unexpectedly high power draw due to high winds, or a miscalculation when planning the mission. It is also possible that the fuel supply fails for because of some unknown issue. It is therefore interesting to see whether the system can effectively switch to battery-only flight, and how much of the battery's capacity can be utilized until total system failure. This will be tested by running the system both with a fully charged battery, and with a battery charged to 50 %, and then turn off the fuel supply, observing the system behaviour.

6.5. Safety and risks

There are some risks associated with experiments where hydrogen gas and highly pressurized containers are involved. A risk analysis was performed prior to practical lab work in order to identify these risks and be able to reduce the probability of them occuring and/or their pontential consequences. See the appendix for more details. Hydrogen gas is flammable

Figure 6.7.: Aerial photo to illustrate the location of the separate gas storage and the lab building. Image credit: Lantmäteriet [48].

in concentrations above 4 % and requires relatively low amounts of energy to ignite [15]. Since there is electronic equipment present in the test cell, there is a risk that sparks could form due to this equipment malfunctioning. The first risk reducing measure was to reduce the possibility of gas collecting locally in the the cell, which could result in dangerous concentration levels. The lab cell was well ventilated and a dedicated ventilation hood was placed above the experiment setup where hydrogen may be present due to leaks or purging of the AeroStak. Electrical equipment was placed physically below the gas connections so that if a leak were to occur, the gas wouldn't be in the proximity of the electronics. Hydrogen is much lighter than air and therefore rises upwards very quickly when released.

A hydrogen sensor was placed within the box, near its ceiling. This sensor gives a signal that is proportional to the hydrogen concentration, or more specifically how close the hydrogen concentration is to the lower explosive limit (LEL). This is the limit for where the hydrogen/air mixture becomes flammable. The LEL for hydrogen is 4 % by volume.

In order to reduce the risk of injuries from the spinning propeller, no person was allowed into the lab cell while tests were performed. The propeller was also placed within a poly carbonate cover to further reduce the probability of someone accidentally touching the propeller.

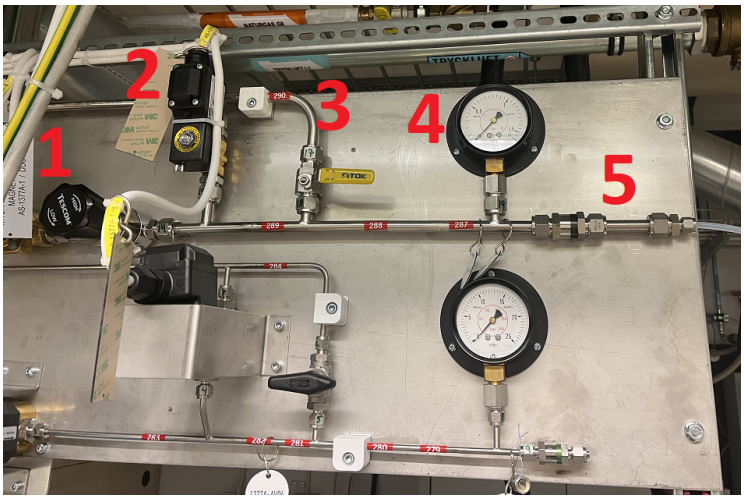

Figure 6.8.: The gas connection board inside the test cell.
1: Pressure regulator.
2: Emergency ventilation solenoid valve.
3: Manual ventilation valve.
4: Pressure gauge, displaying absolute pressure within the tube.
5: Connection to the experiment setup.

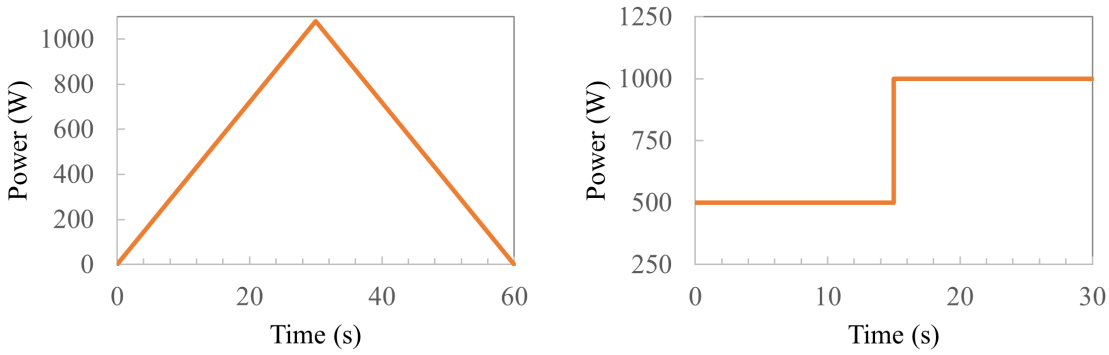

(a) A power sweeping load profile.

(b) A power step load profile.

Figure 6.9.: Two load profiles to be used to test stack load response.

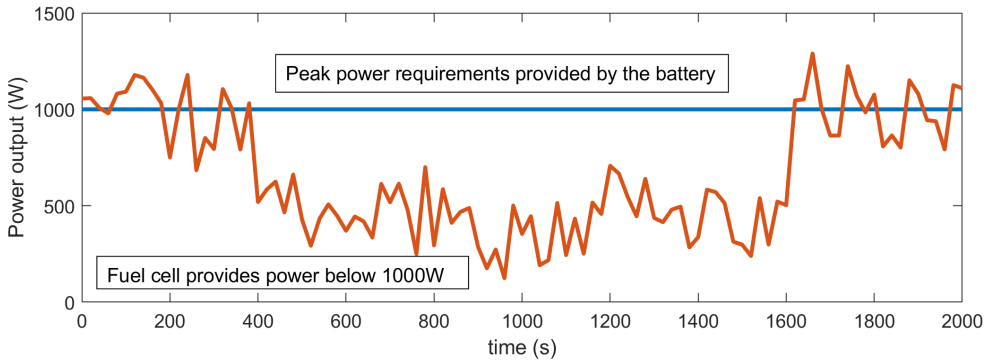

Figure 6.10.: A simulated load cycle for a 30 minute UAV mission. Credit to Rohith Maben at TFHS [16].

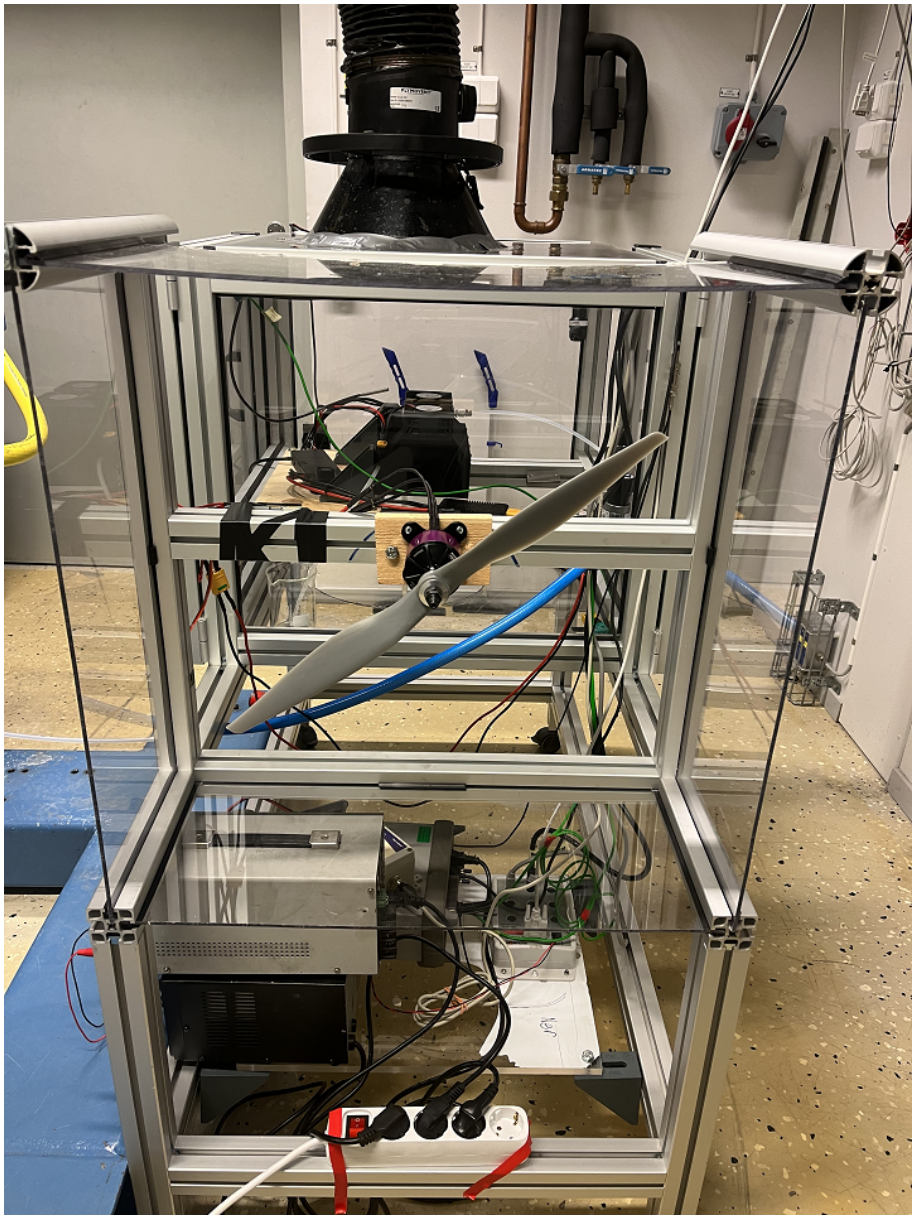

Figure 6.11.: The experiment setup as viewed from the propeller side. Visible around the propeller is the polycarbonate sheets that form an enclosure around the propeller edges. In the background is the fuel cell-containing box with the ventialtion hood in black mounted on top. Power supplies and electronics can be seen below the propeller and fuel cell box.

7. Results

7.1. Pressure issues

The first version of the experiment setup used a pressure regulator located about 2 metres away from the rest of the equipment, and there the gas was regulated to the operating pressure and fed to the fuel cell via PTFE tube. This turned out to cause far too large pressure drops when flow was established in the hose. The 0.8 bar gauge pressure dropped to less than 0.2 when gas was flowing, which is well below the lower operating range of the stack. Gauge pressure refers to the absolute pressure of the gas, minus the atmospheric pressure.

Another issue was found with the pressure regulator itself, as the pressure resolution that it provided proved too rough for accurate experiments. After coming to this comclusion the gas supply was rebuilt and a higher (roughly 6 bar) pressure was kept in the long PTFE tube. A more accurate regulator was put near the fuel cell where the higher pressure was regulated down to operating pressure. To minimize the distance and therefore loss of pressure between the regulator and the fuel cell, one of the two mass flow controllers was removed. Maintaining a higher pressure up until the low pressure regulator means that the pressure drop is lower when there is a flow of gas.

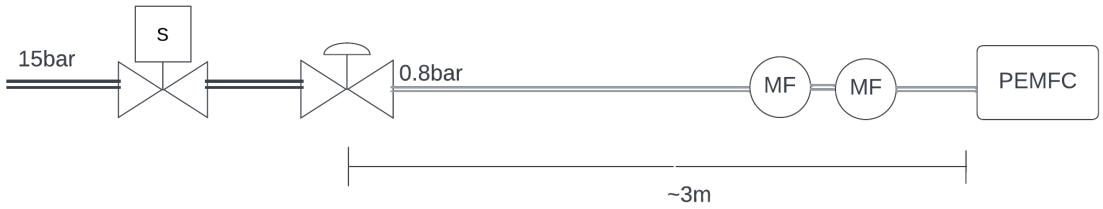

Figure 7.1.: Schematic figure of the first version of the gas connection. The ”S” valve is a solenoid valve. The second valve from the left is a pressure regulator, and the ”MF” devices are the mass flow controllers.

The original point of having an additional mass flow meter was to verify the goodness of the measurements, and to average the two measurements instead of relying on one single set of data. After realizing that it is impossible to know how wrong the measurements are, without a properly calibrated instrument, and that the exactness of the results are not crucial to the experiments to be performed, the author decided that removing one of the two sensors would not compromise the ability to draw conclusions from results. The two mass flow meters gave relatively similar measurements, with transient flows being an exception. There appears to be some form of stationary error in one or both of the devices, since they

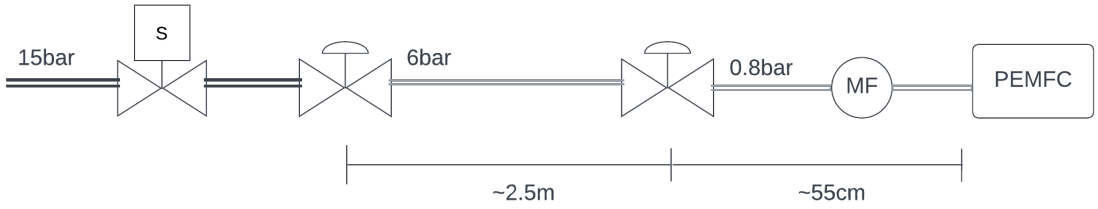

Figure 7.2.: Schematic figure of the rebuilt version of the gas connection

measure slightly different during constant gas flow. See Figure 7.3 for a comparison of the two mass flow meters. The transient gas flow in the beginning results in a large difference, 25 %, between the two measurements. For the more stationary flow, the average difference is about 1 %. Transients similar to the one in the graph are not expected to occur when the fuel cell controls the gas flow, and the overall flow will reach a maximum of 11 SLPM [14].

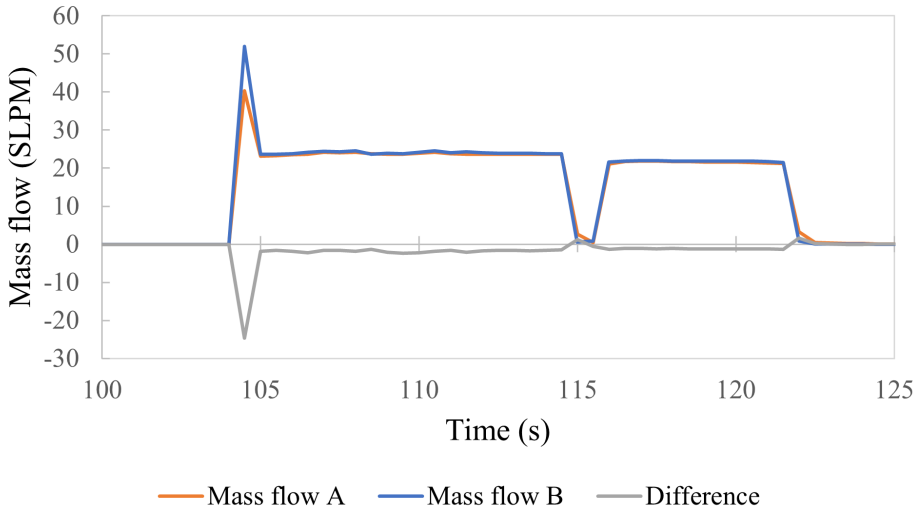

Figure 7.3.: Comparison between the measurements made by mass flow meter A and B on the same flow of gas. The flow was created by manually letting gas exit the quick-connect at the end of the tube. A stationary difference is visible between the two sensors, but it is impossible to say which one of the sensors, or if both, has a measurement error.

7.2. Issues with the fuel cell pressure readings

It was noticed from the first few startups of the AeroStak that something was still wrong with the pressure. Studying the logs produced by the device, it seemed as there was some kind of problem with the integrated pressure sensor. From one of the first runs, there was a log file indicating that the supply pressure was a lot higher than is allowed by the fuel cell. It was not clear if this value is correct, and if it is correct whether it resulted from an operating error while setting the pressure, or from the pressure regulator malfunctioning in some way. In either case, when testing the rebuilt gas connection it was discovered that no pressure readings came from the fuel cell stack. The signal from the pressure sensor is sent to the logic board via a multi-pin connector, and it was thought that this connector could be

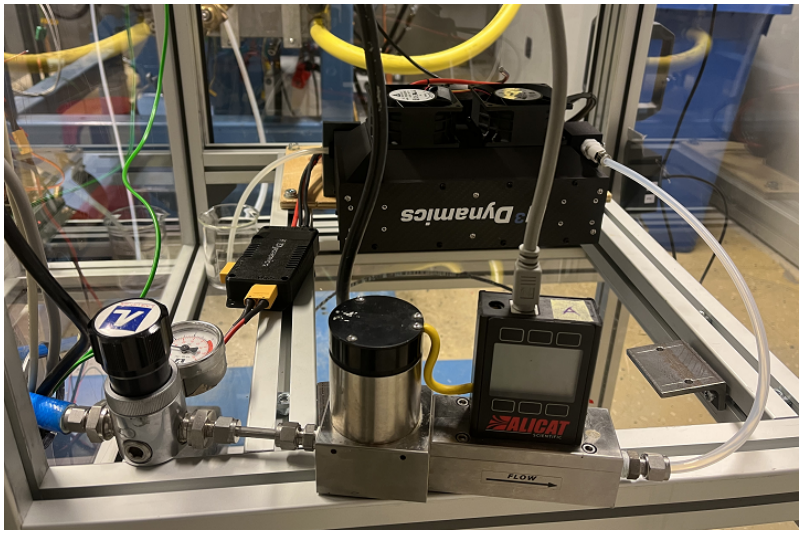

Figure 7.4.: Image of the rebuilt version of the gas connection in the lab. To the left is the pressure regulator with improved resolution in the 0-5 bar range (gauge pressure).

poorly fitted. But even after refitting the connector, the problem with no pressure reading continued. Log files that illustrate this problem can be found in the appendix, Figures A.1, A.2, and A.3.

7.2.1. Testing with the supplied pressure regulator

Thinking that something could be faulty with the gas supply or the pressure regulators at the lab, another test was performed where the pressure regulator supplied by H3Dynamics was used. This regulator is specifically designed to supply a constant pressure within the operating range of the fuel cell. The AeroStak had been tested at the factory with an identical regulator, so the idea was that if this test also failed then issues with the gas supply could be ruled out. The regulator was mounted to one of the 2 liter cylinders and gas connections were fitted to be able to fill the cylinder.

Before first use of the cylinder, it was necessary to perform a purging sequence of the cylinder to ensure that the concentration of air and oxygen was at acceptably low levels before hydrogen was introduced. The reason for this was to avoid the risk of creating an explosive mixture of oxygen and hydrogen within the tank, and to avoid fuel cell poisoning from contaminants present in the cylinder. The purge was performed by filling the tank to 50 bar with an inert gas, in this case nitrogen, and letting the tank slowly empty until the regulator reached its minimal flow rate. This procedure was performed twice. Afterwards, the same procedure was performed once with hydrogen. After this the cylinder was filled to 60 bar with the hydrogen and was ready to provide a steady gas flow via the pressure regulator. It was noted that the 2 liter cylinder could only have been filled to the current pressure of the industrial hydrogen cylinder, thus to reach the maximum capacity of the 2 liter cylinder (300 bar) one would need a higher-pressure fueling tank or a compression system of some kind.

When testing the AeroStak with the 2 liter cylinder and the mounted pressure regulator, the

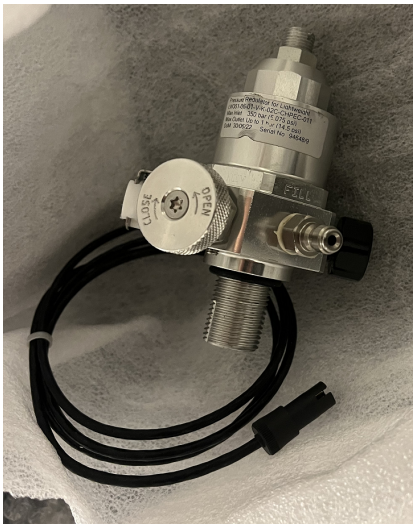

Figure 7.5.: The H3Dynamics-provided hydrogen pressure regulator. Visible is the main valve and the connector for filling. The regulator is threaded in order to be screwed into the hydrogen cylinder.

Figure 7.6.: The 2L cylinder with the pressure regulator mounted.

same issues as previously discussed were still present. Issues with the gas supply could thus be ruled out, but instead there was most likely some kind of problem with the fuel cell pressure sensor. It is possible that a too large pressure was supplied to the stack at some point, which could have damaged the sensor or other hardware. It could also be a faulty electrical connection, but it is currently impossible to know exactly what the problem is.

The main issue was not the fact that the pressure readings weren't logged, but that the fuel cell logic would not allow the startup sequence to complete without an acceptable hydrogen input pressure. This meant that the fuel cell could not function without a working pressure reading.

8. Discussion

8.1. Unresolved fuel cell issues

Since the AeroStak didn't function properly, it was agreed between the manufacturer and the author to ship the device to the factory in the United States where diagnostics and repairs could be performed. Due to issues with the shipping and an already delayed project due to a large delay in the initial delivery of the AeroStak, the device never returned in time for the project deadline, and the experiments could never be performed. The package got to the U.S. but the post office could not contact the receiving party for some reason. This information got sent to an e-mail adress that were not under the supervision of the author leading to further delay. As of finishing this report, the device has yet to return to the lab.

The fact that it was the first time using the gas supply system and the author's first time constructing such an experiment setup meant that most things took a little or a lot longer than expected, leading to the current point in time where there simply is not enough time to continue waiting for the AeroStak to return in a functioning state. A lot of lessons were learned about the reality of performing actual experiments and dealing with hardware in general.

The manufacturer has since communicated that the problems were due to damaged electrical wiring inside the fuel cell casing, which supposedly was caused during manufacturing.

Integration and system perspective

It is possible today to purchase a hybrid hydrogen fuel cell system and a UAV airframe separately and, with some modifications to the fuel cell's physical packaging, mount the system within the airframe. Though this was never done in practice, the models showed that it could be done. The specific hybrid fuel cell system evaluated in this report provides slightly better energy density than a battery-electric alternative would, a 6 % increase. This should result in a similarly-sized range increase compared to the battery-electric system. The difference is very small but the hybrid hydrogen system could be further optimized to improve this number.

An issue with the hybrid fuel cell solution is the bulkiness of the system. It was shown that both the battery-electric and the combustion-based power system provided sufficient power while occupying a much smaller physical volume in the UAV. The volume of the hybrid fuel cell system is a limiting factor for the gravimetric energy density. It is possible to add an additional hydrogen cylinder and stay under the maximum take-off weight, which would provide an additional $\sim$ 700 Wh of energy and a 22 % increase in energy density. This is

however not possible due to space constraints. It should be noted that some of the physical constraints are due to the airframe not being specifically designed to fit hydrogen cylinders. It is possible to get more hydrogen storage per volume unit by using larger cylinders, but then the airframe would need to be modified.

If used to power the Penguin B airframe, it was estimated that the UAV could fly for 3 hours with this hybrid fuel cell system. This could very well be sufficient for the thought-out missions, but it is far less than what is possible with an internal combustion engine. The ICE could fly for over 24 hours with the same system mass. This weight would even become lower as time passes and fuel is burned, resulting in lower power required for cruising and possibly an even longer range. It would depend on the mission requirements whether or not 3 hours of flight is sufficient for the UAV.

A potential problem for hybrid fuel cell systems are cold starts, i.e starting the PEMFC in sub-zero temperatures. Especially in Swedish climate this would be an issue during the winter months. When the system is running at the operating temperature, this is probably less of an issue. But it sets some limitations on when and where start-up's can be performed. Due to the issues that were had, there was no possibility of testing the system performance during cold starts. Apart from the potential issues with temperature, using the hybrid fuel cell system in UAV's seems to be a good idea as the dynamic nature of the loads that are required leads to better fuel cell health than stationary loads.

The fuel cell system requires some off-board infrastructure to refuel. In order to fully fuel the high pressure cylinders to their 300 bar rating, it needs to have access to an industrial cylinder with at least the same pressure, or a compression system for pressurizing gas before refueling. The technology for this is however available.

8.2. Future work

Due to time constraints and a large uncertainty in when the AeroStak repair would be done, the author could not wait for the fuel cell stack to return. Thus, the experiments were never performed. This would be the first thing to finish once the fuel cell stack is returned.

It might be of interest to include high resolution voltage and current measurements in the experiment setup, as this would allow for detailed study of the stack operation characteristics. Especially the stack voltage during load changes and during the purging sequence could be interesting to study.

The project did not (in time) arrive at a stage where the fuel cell system could be integrated into the airframe, but for future work this would be an obvious next step.
When the issues with the AeroStak are resolved, it should be able to power the UAV as planned, which would be very exciting.

Having a fuel cell stack at the department could also be useful for validating physical models of fuel cells. Another interesting project would be to investigate the cold start performance of the fuel cell.

Bibliography

[1] B. Sundén, *Hydrogen, Batteries and Fuel Cells*. London: Academic Press, 2019.

[2] N. Lapeña-Rey, J. Blanco, E. Ferreyra, J. Lemus, S. Pereira and E. Serrot, 'A fuel cell powered unmanned aerial vehicle for low altitude surveillance missions,' *International Journal of Hydrogen Energy*, vol. 42, no. 10, pp. 6926–6940, 2017, ISSN: 0360-3199. DOI: https://doi.org/10.1016/j.ijhydene.2017.01.137. [Online]. Available: https://www.sciencedirect.com/science/article/pii/S0360319917303038.

[3] A. Gong and D. Verstraete, 'Fuel cell propulsion in small fixed-wing unmanned aerial vehicles: Current status and research needs,' *International Journal of Hydrogen Energy*, vol. 42, no. 33, pp. 21 311–21 333, 2017, ISSN: 0360-3199. DOI: https://doi.org/10.1016/j.ijhydene.2017.06.148. [Online]. Available: https://www.sciencedirect.com/science/article/pii/S036031991732503X.

[4] Y. Gao, C. Jausseme, Z. Huang and T. Yang, 'Hydrogen-powered aircraft: Hydrogen–electric hybrid propulsion for aviation,' *IEEE Electrification Magazine*, vol. 10, no. 2, pp. 17–26, 2020.

[5] K. A.-H. S. Njoya Motapon L. -A. Dessaint, 'A comparative study of energy management schemes for a fuel-cell hybrid emergency power system of more-electric aircraft,' *IEEE Transactions on Industrial Electronics*, vol. 61, no. 3, pp. 1320–1334, 2014.

[6] N. Gavrilovic, D. Vincekovic and J.-M. Moschetta, 'A long range fuel cell/soaring uav system for crossing the atlantic ocean,' Oct. 2019.

[7] E. Özbek, G. Yalin, S. Ekici and T. H. Karakoc, 'Evaluation of design methodology, limitations, and iterations of a hydrogen fuelled hybrid fuel cell mini uav,' *Energy*, vol. 213, p. 118 757, 2020, ISSN: 0360-5442. DOI: https://doi.org/10.1016/j.energy.2020.118757. [Online]. Available: https://www.sciencedirect.com/science/article/pii/S0360544220318648.

[8] C. De Wagter, B. Remes, E. Smeur *et al.*, 'The nederdrone: A hybrid lift, hybrid energy hydrogen uav.,' 2020. [Online]. Available: https://ludwig.lub.lu.se/login?url=https://search.ebscohost.com/login.aspx?direct=true&AuthType=ip,uid&db=edsarx&AN=edsarx.2011.03991&site=eds-live&scope=site.

[9] G. Singhal, B. Bansod and L. Mathew, 'Unmanned aerial vehicle classification, applications and challenges: A review,' Nov. 2018. DOI: 10.20944/preprints201811.0601.v1.

[10] ©. C.Stadler/Bwag, *The dji mavic air 2 drone in flight*, CC-BY-SA-4.0, 2021. [Online]. Available: https://commons.wikimedia.org/wiki/File:DJI_-_Drohne_Mavic_Air_2.JPG.

[11] I. Blix, *Dji avata: Fpv-drönaren för vanligt folk*, https://m3.idg.se/2.1022/1.770864/dji-avata, Accessed: 2022-10-24, 2022.

[12] N. G.-A. www.ngphoto.biz, *Elbit systems hermes-450 unmanned aircraft takeoff*, https://upload.wikimedia.org/wikipedia/commons/a/a0/NGP_DSC_0364.jpg, CC BY-SA 3.0, 2011.

[13] T. Morrin, *Choosing the right gas cylinder – type 1, type 2, type 3 or type 4?* https://ams-composites.com/choosing-the-right-gas-cylinder-type-1-type-2-type-3-or-type-4/, Accessed: 2022-12-19, 2022.

[14] H3Dynamics, *Aerostak 1000w hydrogen fuel cell operation & maintenance manual*, R Foundation for Statistical Computing, 67 Ayer Rajah Crescent 23/24, Singapore 139950, 2022.

[15] C. of the desert, 'Hydrogen properties,' p. 15, 2001.

[16] R. Maben, Personal communication, 2022.

[17] *A60-5s v4 28-pole kv295*, https://hackermotors.us/product/a60-5s-v4-28-pole-kv295/, Accessed: 2022-10-27.

[18] L. Khotseng, 'Fuel cell thermodynamics,' in *Thermodynamics and Energy Engineering*, P. Vizureanu, Ed., Rijeka: IntechOpen, 2019, ch. 1. DOI: 10.5772/intechopen.90141. [Online]. Available: https://doi.org/10.5772/intechopen.90141.

[19] K. Harrison, R. Remick and G. Martin, 'Hydrogen production: Fundamentals and case study summaries,' in *Proc. of the 18th World Hydrogen Energy Conference*, ser. WHEC, Essen, Germany: NREL, 2010.

[20] Engineering Toolbox, *Atmospheric pressure vs. elevation above sea level*, https://www.engineeringtoolbox.com/air-altitude-pressure-d_462.html, Accessed: 2022-12-19, 2003.

[21] Engineering Toolbox, *U.s. standard temperature vs. altitude*, https://www.engineeringtoolbox.com/standard-atmosphere-d_604.html, Accessed: 2022-12-29.

[22] T. Hordé, P. Achard and R. Metkemeijer, 'Pemfc application for aviation: Experimental and numerical study of sensitivity to altitude,' *International Journal of Hydrogen Energy*, vol. 37, no. 14, pp. 10 818–10 829, 2012, ISSN: 0360-3199. DOI: https://doi.org/10.1016/j.ijhydene.2012.04.085. [Online]. Available: https://www.sciencedirect.com/science/article/pii/S0360319912009391.

[23] B. Pollet, A. Franco, H. Su, H. Liang and S. Pasupathi, '1 - proton exchange membrane fuel cells,' in *Compendium of Hydrogen Energy*, ser. Woodhead Publishing Series in Energy, F. Barbir, A. Basile and T. N. Veziroğlu, Eds., Oxford: Woodhead Publishing, 2016, pp. 3–56, ISBN: 978-1-78242-363-8. DOI: https://doi.org/10.1016/B978-1-78242-363-8.00001-3. [Online]. Available: https://www.sciencedirect.com/science/article/pii/B9781782423638000013.

[24] A. G. Olabi, T. Wilberforce, A. Alanazi *et al.*, 'Novel trends in proton exchange membrane fuel cells.,' *Energies (19961073)*, vol. 15, no. 14, N.PAG, 2022, ISSN: 19961073. [Online]. Available: https://ludwig.lub.lu.se/login?url=https://search.ebscohost.com/login.aspx?direct=true&AuthType=ip,uid&db=a9h&AN=158210179&site=eds-live&scope=site.

[25] A. Hermann, T. Chaudhuri and P. Spagnol, 'Bipolar plates for pem fuel cells: A review,' *International Journal of Hydrogen Energy*, vol. 30, no. 12, pp. 1297–1302, 2005, Cancun 2003, ISSN: 0360-3199. DOI: https://doi.org/10.1016/j.ijhydene.2005.04.016. [Online]. Available: https://www.sciencedirect.com/science/article/pii/S0360319905000935.

[26] S. Asghari, M. Shahsamandi and M. Ashraf Khorasani, 'Design and manufacturing of end plates of a 5kw pem fuel cell,' *International Journal of Hydrogen Energy*, vol. 35, no. 17, pp. 9291–9297, 2010, ISSN: 0360-3199. DOI: https://doi.org/10.1016/j.ijhydene.2010.02.135. [Online]. Available: https://www.sciencedirect.com/science/article/pii/S0360319910004428.

[27] H3Dynamics, *Hydrogen air mobility power solutions and accessories*, https://www.h3dynamics.com/_files/ugd/3029f7_db7f1517df744509b837916c4d939ae3.pdf, Accessed: 2022-10-27, 2021.

[28] D. Qiu, L. Peng, P. Yi, W. Lehnert and X. Lai, 'Review on proton exchange membrane fuel cell stack assembly: Quality evaluation, assembly method, contact behavior and process design,' *Renewable and Sustainable Energy Reviews*, vol. 152, p. 111 660, 2021, ISSN: 1364-0321. DOI: https://doi.org/10.1016/j.rser.2021.111660. [Online]. Available: https://www.sciencedirect.com/science/article/pii/S1364032121009357.

[29] R. Omrani, S. Seif Mohammadi, Y. Mafinejad, B. Paul, R. Islam and B. Shabani, 'Pemfc purging at low operating temperatures: An experimental approach,' *International Journal of Energy Research*, vol. 43, no. 13, pp. 7496–7507, 2019. DOI: https://doi.org/10.1002/er.4783. eprint: https://onlinelibrary.wiley.com/doi/pdf/10.1002/er.4783. [Online]. Available: https://onlinelibrary.wiley.com/doi/abs/10.1002/er.4783.

[30] B. Belvedere, M. Bianchi, A. Borghetti, A. De Pascale, M. Paolone and R. Vecci, 'Experimental analysis of a pem fuel cell performance at variable load with anodic exhaust management optimization,' *International Journal of Hydrogen Energy*, vol. 38, no. 1, pp. 385–393, 2013, European Fuel Cell 2011, ISSN: 0360-3199. DOI: https://doi.org/10.1016/j.ijhydene.2012.09.147. [Online]. Available: https://www.sciencedirect.com/science/article/pii/S0360319912022148.

[31] Y. Luo and K. Jiao, 'Cold start of proton exchange membrane fuel cell,' *Progress in Energy and Combustion Science*, vol. 64, pp. 29–61, 2018, ISSN: 0360-1285. DOI: https://doi.org/10.1016/j.pecs.2017.10.003. [Online]. Available: https://www.sciencedirect.com/science/article/pii/S0360128517300175.

[32] T. Gießgen and T. Jahnke, 'Assisted cold start of a pemfc with a thermochemical preheater: A numerical study,' *Applied Energy*, vol. 331, p. 120 387, 2023, ISSN: 0306-2619. DOI: https://doi.org/10.1016/j.apenergy.2022.120387. [Online]. Available: https://www.sciencedirect.com/science/article/pii/S0306261922016440.

[33] L. Lei, P. He, P. He and W.-q. Tao, 'Numerical research on the cold start-up strategy of a pemfc stack from 30°c,' *Journal of Thermal Science*, Oct. 2022, ISSN: 1993-033X. DOI: 10.1007/s11630-022-1712-8. [Online]. Available: https://doi.org/10.1007/s11630-022-1712-8.

[34] M. Jourdan, H. Mounir and A. El Marjani, 'Compilation of factors affecting durability of proton exchange membrane fuel cell (pemfc),' in *2014 International Renewable and Sustainable Energy Conference (IRSEC)*, 2014, pp. 542–547. DOI: 10.1109/IRSEC.2014.7059906.

[35] S. Kreitmeier, G. A. Schuler, A. Wokaun and F. N. Büchi, 'Investigation of membrane degradation in polymer electrolyte fuel cells using local gas permeation analysis,' *Journal of Power Sources*, vol. 212, pp. 139–147, 2012, ISSN: 0378-7753. DOI: https://doi.org/10.1016/j.jpowsour.2012.03.071. [Online]. Available: https://www.sciencedirect.com/science/article/pii/S0378775312006921.

[36] Ž. Penga, G. Radica, F. Barbir and P. Eckert, 'Degradation mechanisms in automotive fuel cell systems,' EU Fuel Cells and Hydrogen Joint Undertaking, Avenue de la Toison d' Or 56- 60, 1060 Brussels, Tech. Rep., Dec. 2017.

[37] P. Gazdzicki, J. Mitzel, D. G. Sanchez *et al.*, 'Operando and ex-situ investigation of pemfc degradation,' *ECS Transactions*, vol. 92, no. 8, p. 261, Jul. 2019. DOI: 10.1149/09208.0261ecst.

[38] Y. Ao, S. Laghrouche, D. Depernet and K. Chen, 'Lifetime prediction for proton exchange membrane fuel cell under real driving cycles based on platinum particle dissolve model,' *International Journal of Hydrogen Energy*, vol. 45, no. 56, pp. 32 388–32 401, 2020, ISSN: 0360-3199. DOI: https://doi.org/10.1016/j.ijhydene.2020.08.188. [Online]. Available: https://www.sciencedirect.com/science/article/pii/S0360319920332158.

[39] P. Pei, Y. Meng, D. Chen, P. Ren, M. Wang and X. Wang, 'Lifetime prediction method of proton exchange membrane fuel cells based on current degradation law,' *Energy*, vol. 265, p. 126 341, 2023, ISSN: 0360-5442. DOI: https://doi.org/10.1016/j.energy.2022.126341. [Online]. Available: https://www.sciencedirect.com/science/article/pii/S0360544222032273.

[40] M. Loganathan, P. Manivannan and A. Ramesh, 'Investigations on performance and emissions of a two-stroke si engine fitted with a manifold injection system,' *Indian Journal of Engineering and Materials Sciences*, vol. 13, no. 2, pp. 95–102, 2006. [Online]. Available: https://www.scopus.com/inward/record.uri?eid=2-s2.0-33749182207&partnerID=40&md5=a51ea884f7b0943a2e7672bffda98960.

[41] *Maxamps 46000mah lipo battery*, https://maxamps.com/collections/9s-lipo-battery-33-3v/products/lipo-46000-9s-33-3v-battery-pack, Accessed: 2023-02-01.

[42] *A60-5s v4 28-pole kv295*, https://skypower.online/produkt/sp-28-cr/, Accessed: 2022-10-27.

[43] *Du-bro fuel tanks*, https://www.dubro.com/products/fuel-tanks?variant=27880844231, Accessed: 2022-10-27.

[44] X. Zhou, T. Yang, J. Xiao, P. Bénard and R. Chahine, 'Estimation of filling time for compressed hydrogen refueling,' *Energy Procedia*, vol. 158, pp. 1897–1903, 2019, Innovative Solutions for Energy Transitions, ISSN: 1876-6102. DOI: https://doi.org/10.1016/j.egypro.2019.01.438. [Online]. Available: https://www.sciencedirect.com/science/article/pii/S1876610219304618.

[45] H3Dynamics, *Electric boost compressor*, https://www.h3dynamics.com/_files/ugd/3029f7_8af73b06f4d441c78c39c367c8b67418.pdf, Accessed: 2023-01-17, 2021.

[46] S. Petrovic, *Battery Technology Crash Course. A Concise Introduction.* Springer International Publishing, 2021, ISBN: 9783030572686. [Online]. Available: https://ludwig.lub.lu.se/login?url=https://search.ebscohost.com/login.aspx?direct=true&AuthType=ip,uid&db=cat02271a&AN=atoz.ebs26991296e&site=eds-live&scope=site.

[47] Alicat, *Operating principle: Laminar differential pressure mass flow technology*, https://www.alicat.com/choosing-an-instrument/theory-of-operation-laminar-differential-pressure-flow-measurement/, Accessed: 2022-01-04.

[48] Lantmäteriet, *Min karta [map]*, https://minkarta.lantmateriet.se/, Accessed: 2023-01-16, 2023.

A. Pressure reading logs

```
DB3:FCSPressure valid, 2.05
DB3:Open waterValve for 100ms
DB3:HGSPressure drops -0.0bar when WaterValve open
DB3:Open valve1, close valve2 for 0.5s
DB3:Close valve1, open valve2 for 1s
...  ,32.8,00.4,32.8,19.6,19.6,20.0,20.0,00.0,019.5,2.05, ...
DB1:E101
DB3:FCSPressure invalid
```

Figure A.1.: Log output from the AeroStak, November 30. Highlighted in bold text is the data field that gives the stack pressure reading. The supplied pressure appears to be larger than is allowed by the fuel cell.

```
DB3:FCSPressure valid, 0.95
...  ,32.4,00.1,32.5,17.9,17.9,20.0,20.0,00.0,018.1,0.00, ...
DB1:PS2 low, 0.00
DB3:System shutdown:  Startup Sensor Check
```

Figure A.2.: A log from December 6. Now no pressure reading is registered. It is not why clear why there is a difference in which lines of data are printed by the AeroStak compared to the first log. The open/close valve lines do not appear in this second log file.

```
DB3:FCSPressure valid, 0.94
...  ,32.5,00.2,32.5,19.0,19.0,20.0,20.0,00.0,019.2,0.00, ...
DB1:PS2 low, 0.00
DB3:System shutdown:  Startup Sensor Check
```

Figure A.3.: A third log where still no pressure reading is registered, even after ensuring that electrical connectors are firmly in place. December 7.

B. Hardware specifications

Here follows complete specifications of the fuel cell stack, the LiPo battery back, and the type III tanks.

Table B.1.: Fuel cell specifications

AeroStak 1000 LV	
Weight	2.30 kg
Geometry	279x127x143 mm
Nominal power	1000 W
Peak power	1299 W
No. of cells	50
Voltage	30.0 V–47.5 V
Current	0 A–35 A
Ambient airtemp	0 °C–35 °C
Fuel pressure	0.6–0.8 bar
El. efficiency (LHV)	56.5 % @ 1080 W

Table B.2.: Hydrogen tank specifications

HES F2 tanks	
Empty weight	1.58 kg
Volume	2 l
Hydrogen mass	42 g
Diameter	114 mm
Length	371 mm
Max pressure	300 bar
Pressure regulator mass	0.305 kg

Table B.3.: Battery pack specifications

LiPo Battery	
Weight	1,094 kg
Geometry	138 x 45 x 83.25 mm
Cell configuration	9 s
C charging	175
C discharging	5
Capacity	5200 mAh
Nominal voltage	33.3 V
Total energy	173 Wh

C. LabView block diagram

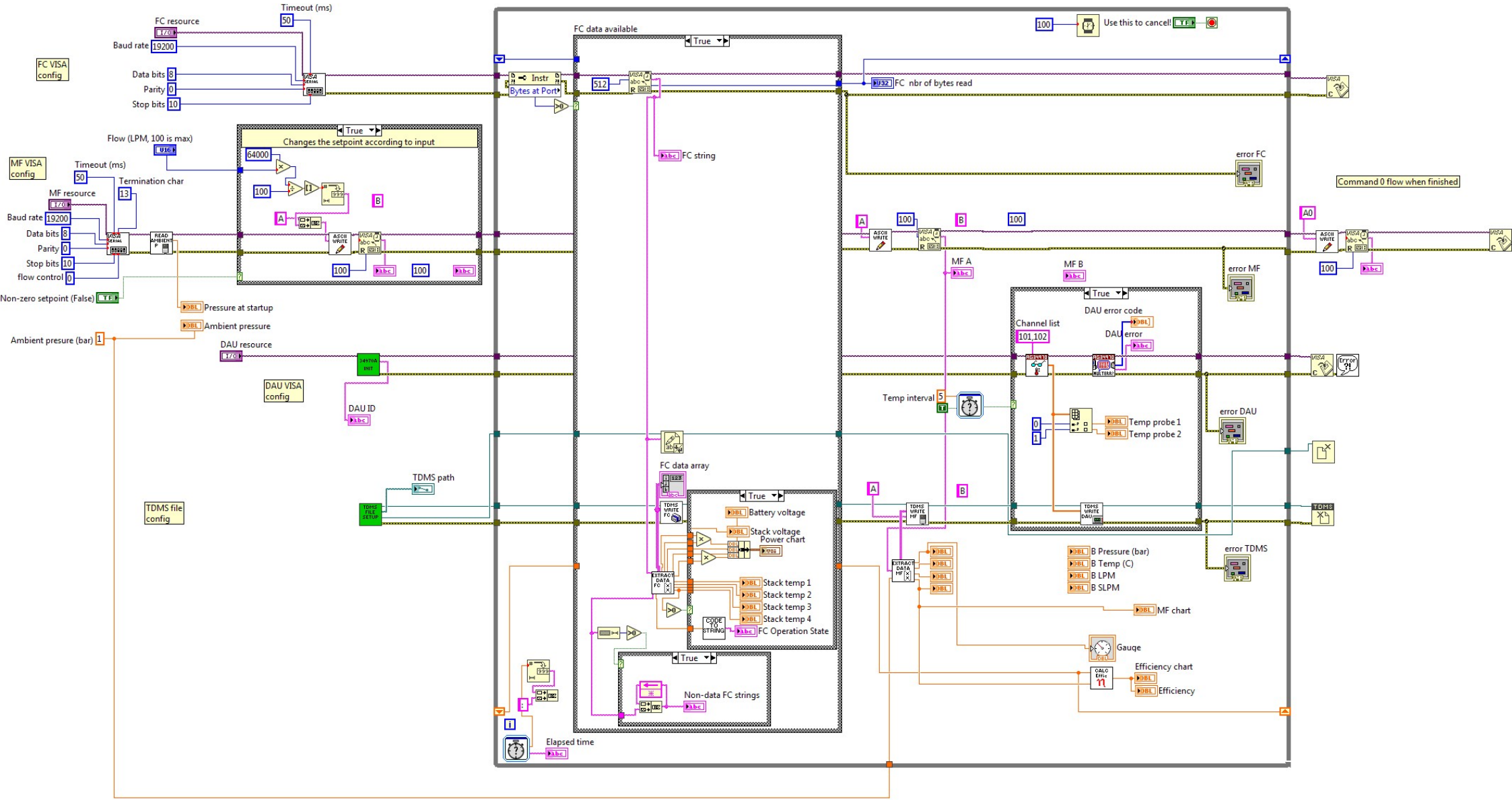
FC VISA config
FC resource
Timeout (ms)
50
Baud rate
19200
Data bits
8
Parity
0
Stop bits
10
MF VISA config
MF resource
Timeout (ms)
50
Termination char
13
Baud rate
19200
Data bits
8
Parity
0
Stop bits
10
flow control
0
Non-zero setpoint (False)
Flow (LPM, 100 is max)
Changes the setpoint according to input
64000
100
Pressure at startup
Ambient pressure
Ambient presure (bar)
1
DAU resource
DAU VISA config
DAU ID
TDMS path
TDMS file config
FC data available
Instr
Bytes at Port
512
FC string
FC data array
Battery voltage
Stack voltage
Power chart
Stack temp 1
Stack temp 2
Stack temp 3
Stack temp 4
FC Operation State
Non-data FC strings
Elapsed time
Use this to cancel!
FC nbr of bytes read
error FC
Command 0 flow when finished
MF A
MF B
error MF
DAU error code
Channel list
101,102
DAU error
Temp interval
5
Temp probe 1
Temp probe 2
error DAU
error TDMS
B Pressure (bar)
B Temp (C)
B LPM
B SLPM
MF chart
Gauge
Efficiency chart
Efficiency

D. Risk assessment

A risk assessment was performed prior to any experimental work. Risks and their expected consequences were identified and their severity and likelihood of occuring were quantified with a scale from 1-3. Risk reducing measures were then decided on in order to keep the product of $risk \times consequence$ at acceptable levels. Attached is the initial risk identification, the risk reducing measures, and a risk assessment matrix that illustrates how the severity of the risks are quantified.

RISK IDENTIFICATION

Make an inventory of risks and scenarios with unwanted consequences associated with the experiment. When identifying risks, it can be helpful to complete the sentence "there is a risk that". Identify the different risks and their positions in the figure of the lab layout shown in the summary.

RISK NO.	TYPE	ACTIVITY/ CAUSE	RISK / ATTRIBUTE	POSITION in Figure or other	P	C	RISK ESTIMATION = PxC
1	Fire	Always	Hydrogen leakage	In storage (4)	1	1	1
2	Fire	During operation	Hydrogen leakage	H2 connections (2,3)	1	2	2
3	Mechanical	During operation	Cutting/Body injury	Propeller (1)	2	3	6
4	Mechanical breakdown	During operation	Flying parts	Propeller (1)	1	3	3
5	Explosion/fire	During operation	Fuel cell failure	Fuel cell	1	3	3
6	Explosion/fire	While electricity is connected	Sparks from electric components	Electrics on test bench (1,2,5,6,7)	1	3	3
7	Explosion	Handling of gas cylinders	Gas cylinder breakage due to physical impact	Gas storage	2	3	6

Comments about the risk identification performed above:

Leakage would most likely occur at the connection points in the gas supply system. The connection between gas supply and experiment setup possibly being the most critical. At hydrogen concentrations above 4%, the gas/air mixture is flammable and require a relatively small amount of energy to ignite.

The propeller will be spinning at several thousand RPM. If its attachment breaks the propeller could launch. If the propeller itself breaks its debris would scatter at high speeds.

RISK REDUCING MEASURES

Go through all identified risks and state the precautions and safety equipment used to PREVENT or REDUCE the different risks.

			After reducing measures		
RISK NO.	**TYPE**	**RISK REDUCING MEASURES**	**P**	**C**	**RISK ESTIMATION = PxC**
1	Hydrogen leakage, fire	1. Hydrogen flasks should be closed after use. 2. Gas storage is ventilated	1	2	2
2	Hydrogen leakage, fire	1. Gas alarm in building detects hydrogen and starts gas alarm. 2. Hydrogen detector in test cell detects leaks and shuts off hydrogen supply from the gas storage. 3. Ventilation in the lab cell is always running while performing experiment. 4. Hydrogen detector is placed above hydrogen connectors and is monitored when gas supply is active.	1	2	2
3	Mechanical	1. Propeller is placed in a metal cage to make accidental contact impossible. 2. Nobody allowed in the lab cell while running the experiment.	1	3	3
4	Mechanical breakdown	1. Propeller is placed within polycarbonate casing. 2. No nylon hoses for hydrogen are placed near or above propeller. 3. Part of hose closest to the propeller is protected with a thick rubber hose.	1	2	2
5	Explosion/fire	1. Fuel cell error codes warns operator of operation anomalies. 2. Fuel cell shuts down automatically when temperature is too high or cell voltage is too low.	1	2	2
6	Explosion/fure	1. AC components i.e. logger, power supply, and power strip, are placed physically below fuel line and its connections.	1	1	1
7	Explosion	1. Gas cylinders are physically restricted from falling 2. Handling of cylinders is limited to bare minimum.	1	3	3

Comments regarding the risk reducing measures and new risk assessment:
The ventilation system should always be running when performing experiments.
Keep away from the moving propeller.
Follow protocol when handling hydrogen.
If the level of hydrogen in the air increases notably, the gas supply should be disconnected and the experiment aborted.

Risk assessment matrix

Low and moderate risks are normally acceptable, while high and very high risks are not. However, while statistics can sometimes be helpful, they can also be misleading – common sense has an important role too.

Below is the "Risk assessment matrix" and the tables

Risk = Probability x Consequence		**Low 1**	**Medium 2**	**High 3**
Probability	**High 3**	Medium risk 3	High risk 6	High risk 9
	Medium 2	Low risk 2	Medium risk 4	High risk 6
	Low 1	Low risk 1	Low risk 2	Medium risk 3

Consequence rating	**Consequence example**
Low (1)	Risk that can cause insignificant or rapid transient illness/damage to person, organization, environment or property.
Medium (2)	Risk that can cause significant illness/injury (first aid treatment) to a person, organization, environment or property.
High (3)	Risk that can cause serious and/or permanent illness/ injury to a person (sick leave/permanent injury), organization, environment or property or alternatively significant risk that occurs frequently.

Probability rating	**Probability definition**
Low (1)	Expected to occur within or has occurred once in the past 10 years. Conceivable, but more likely not to happen than happen.
Medium (2)	Expected to occur several times in the past 10 years.
High (3)	Expected to occur or has occurred at least once a year.

RISK ESTIMATION = Probability x Consequence

Risk Estimation value 1-2: Low risk **– Awareness/ information needed, acceptable as is**
Risk Estimation value 3-5: Moderate risk **- Should be reduced, acceptable with high awareness**
Risk Estimation value 6-9: High risk – **Action needed, must be reduced**